By Enough, But Not Too Much

Where the Twist Is the Floor of the Yang–Mills Hessian on Berger Spheres

Bee Rosa Davis
Davis Geometric
ORCID 0009-0009-8034-4308

November 2026 (version 1.1)

Abstract. On the Berger spheres $(t, 1, 1)$, every left-invariant $SU(2)$ field that is invariant under the right rotation about the long circle, lifted by a constant gauge circle, is, up to constant gauge, $M_0 = x\,\tau_0$, $M_1 = y\,\tau_1$, $M_2 = y\,\tau_2$: a strength x along the long circle and a strength y across it. At every such field the twist $f\,(\hat\theta^1 + i\hat\theta^2)\otimes(\tau_1 + i\tau_2)$ is an exact gauge-orthogonal eigenvector of the Yang–Mills Hessian in the sector of spin $j/2$, with eigenvalue $(x + (j+2)/\sqrt{t})^2 + 2\sqrt{t}\,x - y^2$. An exact symbolic Weitzenböck identity, proved for the whole family, gives the charge blocks of $H + GG^*$ in closed form. The set of x where the twist is the floor of every sector is bounded on both sides. In both spectra it lies in $[r_{\mathrm{lo}}, r_{\mathrm{hi}}]$, set by a state of the sector $j = 0$ (proved). For $H + GG^*$ it also lies in $x \le \min(x_{12}^*, 0)$, with x_{12}^* its upper end in the sectors $j \le 12$, because for $x > 0$ high sectors undercut the twist (proved for $H + GG^*$; computed for the gauge-orthogonal spectrum), and above the smallest root of an explicit cubic from the sector-0 block of charge ± 1 (proved). On every grid computed it is one interval (computed). Where the charge-0 block of the sector $j = 4$ competes, the edge computed in the sectors $j \le 12$ is a root of an explicit factor P_2 of degrees 7, 8 and 16 in x, y and $\sqrt{t}$. Its restriction to the Berger path contains the polynomial of the threshold t_A of the Floor paper, and these identities are also checked in Lean 4. On the domain $x \in [-3, -1.5]$, $y \in [0.5, 3]$, $t \in [3, 10]$, interval certificates prove that the twist is the floor of every sector, with multiplicity two, with the certificates' rows proved equal to the operator's. The all-sector edge of $H + GG^*$ is at most $\min(x_{12}^*, 0)$; equality is conjectured for $t \ge 3$ and fails at and near $t = 2$. Three simpler readings, each written down before its data, failed. Six further tests were pre-registered. At 48 new points the region in the sectors $j \le 12$ is one interval on a 0.01 grid, no sector $13 \le j \le 79$ undercuts the twist at the three tested values of $x < 0$, and the edge is the P_2 root at 34 of 38 points. At 193 random circle-symmetric fields the region in $j \le 12$ is again one interval, but the reading that the competitor is nearly blind to x fails at 129. In an $SU(3)$ family stretched along the hypercharge circle with a free fibre field, the twist is the floor of all nine tested sectors at no x of the 0.25 scan, at any of 20 shapes. Stretched instead along the twist's own charge circle, the same group gives her back: she is the floor at 19 of 20 shapes, in one interval, on the side where the field along her circle turns against her charge. For $x > 0$ the floor of every sector is held, from small j on, by a state that turns against the field (60 of 60 points). Swept across the Weyl chambers of $SU(4)$ and $Sp(2)$, she lives on the coroot of her own highest root, not on the principal circle.

Keywords. Yang–Mills Hessian; Berger sphere; Peter–Weyl decomposition; Weitzenböck identity; spectral gap; level crossing; computer-assisted proof; formal verification.
MSC 2020. 58J50, 81T13, 58E15, 53C30, 65G30, 03B35.

Helike, in plain words

A gauge field on a curved space can be disturbed in many directions. Some disturbances cost energy and some release it. The Yang–Mills Hessian keeps the account of those costs: each of its

eigenvalues is the cost of one way of disturbing the field.

The space here is a three-sphere stretched along one family of circles, a Berger sphere. It has one long direction, along those circles, and two short directions across them. How much it is stretched is a single number, t.

Helike is one particular disturbance, which I call *the twist*. She turns in the two short directions of space, and in step with them she turns in two internal directions of the gauge field. Because space and the internal directions turn together, she carries a definite charge under the rotation about the long circle. She is the only disturbance with that much charge, so she cannot mix with anything, and her cost can be written down exactly. The disturbances come in sectors, from coarse ($j = 0$) to finer and finer variation over the sphere, and she has a copy in every sector.

The *floor* is the cheapest way to disturb the field: the lowest eigenvalue of the Hessian. In my earlier paper [6] Helike is the floor of every sector at one particular field, the Berger field, for stretches from $t = 2.75$ to $t = 10$. In this paper the field around her is allowed to change. It has a strength x along the long circle and a strength y across it. The question is where in that family she is still the cheapest disturbance, in every sector at once.

What I find is a band. Her cost has an exact formula. Lifting her from one sector to the next carries a discount, $2xj/\sqrt{t}$, and it is a discount only when $x < 0$, that is, when the field along her own circle turns against her charge. If it does not turn against her by enough, some other disturbance in some sector becomes cheaper than her: that is the upper edge. If it turns against her by too much, her cost in the coarsest sector grows like x^2, while some disturbances there do not get more expensive, and one of them undercuts her: that is the lower edge. So she is the floor only by enough, but not too much. What is proved: the band is bounded on both sides, positive x loses (for the operator $H + GG^*$), and on one box of fields she is the floor of every sector. What is computed: on every grid I have scanned, the band is one interval.

My reading. I read this paper as a study of what Helike does when the field around her changes. At the Berger field she shows up as the floor; here I follow her as the field moves, and she keeps the same shape and the same exact eigenvalue formula while her standing as the floor depends on the field along her own circle. That is my reading, not a theorem. The $SU(3)$ test of Section 8 (Test C) is a check on it: in an $SU(3)$ family stretched along the hypercharge circle she is the floor of the tested sectors nowhere on the scan, so the behaviour found here does not carry over to every setting I have tested. Stretched instead along her own charge circle (Test D), the same group gives her back, at 19 of 20 shapes. So in $SU(3)$ the circle decides. A further test (Test F) sweeps the circle across the chambers of $SU(4)$ and $Sp(2)$: she lives on the circle of her own $SU(2)$ and just inside it, and not on the principal circle.

1 Introduction

The second variation of the Yang–Mills energy says which directions at a gauge field lead downhill and which lead up. In [6] I computed it at the *Berger field*, the Levi-Civita connection of the Berger metric $(t, 1, 1)$ on $S^3 = SU(2)$ read as an $SU(2)$ connection. In every Peter–Weyl sector j (spin $j/2$) the field $b = f\,(\hat{\theta}^1 + i\hat{\theta}^2) \otimes (\tau_1 + i\tau_2)$, with f the top weight along the long axis, is an exact eigenvector of the Hessian, orthogonal to every gauge direction, with eigenvalue

$$\lambda_t(j) = \frac{j(j+2) - 2(t-3)j - 2(t-2)(t+4)}{t}.$$

I call this field Helike ("she who turns"); below it is *the twist*. The paper [6] proved that $\lambda_t(j)$ is the lowest eigenvalue of every sector for every $t \in [2.75, 10]$. Below that range it found, in double precision, that the floor is lost below $t^* \approx 2.6980$ for the gauge-orthogonal spectrum and below the algebraic threshold $t_A = 2.73112227823811362\ldots$ for $H + GG^*$.

The Berger field is one point of a larger family. This paper asks where in that family the twist is the floor, and what sets the edge of that region. Stability of Yang–Mills fields on spheres and homogeneous spaces is classical [5, 15, 21, 14], results for minimal-energy Yang–Mills connections on three-manifolds of nonnegative Ricci curvature are in [23], and a recent quantitative upper bound for the lowest Hessian eigenvalue of abelian Yang–Mills–Higgs critical points on the round S^3 is [11]. Those results concern critical points. The fields here are in general not critical points. On Berger spheres, spectra are known for the scalar Laplacian [16], the Dirac operator [3, 13] and the Hodge Laplacian on 1-forms [10]; Bär's computation [3] uses Frobenius reciprocity, the same sector decomposition used here.

Main results. Section 2 fixes the operator and the family $M_0 = x\tau_0$, $M_1 = y\tau_1$, $M_2 = y\tau_2$. Each result carries a status: proved (exact symbolic computation or rigorous interval arithmetic), computed (double precision), or proved under (T), where the proof runs through a code transcription of the proved rows that is checked in double precision (Section 2.4).

- *The family is general* up to constant gauge, within the class of left-invariant fields invariant under the right rotation about the long circle lifted by a constant gauge circle (Proposition 2.1).
- *The Weitzenböck identity and the charge blocks* (Lemmas 2.2 and 2.3; proved): $H + GG^* = \sum_i X_i^* X_i + R_0$ holds exactly for the whole family, and a conserved charge splits every sector into blocks of at most nine states, with rows in closed form in (x, y, t).
- *The twist across the family* (Section 3; proved): its eigenvalue is $\lambda = (x+(j+2)/\sqrt{t})^2+2\sqrt{t}\,x-y^2$ (Proposition 3.2). The cost of lifting it from sector 0 to sector $j \geq 1$ carries a discount $2xj/\sqrt{t}$, negative if and only if $x < 0$ (Corollary 3.3). Its anatomy is exact: fibre momentum squared, a lowest-Landau-level transverse term, and a curvature term (Proposition 3.4).
- *The edge polynomial* (Section 4): the determinant for the charge-0 block of sector 4 factors as $-16384\,P_1P_2$ (Proposition 4.1; proved), and on the Berger path $P_2 = -32(s-1)(s+1)Q_{16}(s)$ with Q_{16} the polynomial of t_A (Proposition 4.2; proved, a polynomial identity). Both identities, and a bracket for the crossing, are checked in Lean 4: sixteen theorems in all (Section 4.6).
- *For $x > 0$ the twist is never the lowest eigenvalue of $H+GG^*$ in every sector*; high sectors undercut it (Theorem 5.1; proved for $H + GG^*$, computed for the gauge-orthogonal spectrum).
- *The region is bounded below.* In both spectra it lies in $[r_{\mathrm{lo}}, r_{\mathrm{hi}}]$, from the sector-0 state $\hat{\theta}^0 \otimes \tau_0$ (Proposition 5.3; proved). For $H + GG^*$ the sector-0 block of charge ± 1 gives a sharper bound, the smallest root of an explicit cubic (Proposition 5.4; proved). That the region is one interval is computed.
- *An exact "if and only if"* for $H + GG^*$ in the sectors $j \leq 12$ on two slices ($t = 3$ with $y = \sqrt{3}$ and with $y = 3/2$), for $x \in [-3, r_{\mathrm{next}})$ (Theorem 5.6; proved under (T)).

- *Large-sector slab proofs* for every sector $j \geq 40$ (Theorem 5.7; PROVED under (T)), on boxes whose top lies about 0.1 below, and in every t-slab also about 0.02 below, the smallest grid value of $\min(x_{12}^*, 0)$ in that slab, and up to $x = -0.02$ on $y \in [1, 3]$, $t \in [7, 10]$ (the distances are measured at grid points, not proved).
- *The floor on a domain* $D = \{x \in [-3, -1.5],\ y \in [0.5, 3],\ t \in [3, 10]\}$, every sector, by interval certificates (Theorem 6.1; PROVED).

The theorem on D also appears, as Theorem 7.3, in the version 3 draft of [6].

WHAT IS COMPUTED. In double precision: tables of the edge in the sectors $j \leq 12$, a map of the eight charge blocks that set it (Section 4.5), and the region on grids (Figure 3). Along the Berger path the $H + GG^*$ edge is crossed within 8×10^{-16} of t_A, and the gauge-orthogonal edge at t^* to about 10^{-12}, the precision of both computations (Section 4.4). Every positive $H + GG^*$ edge found within $j \leq 12$ is an artefact of the cut-off: at all 58 such grid points a higher sector undercuts the twist (Section 5).

WHAT FAILED. Three readings were tested, each written down before its data, and each failed: that the rotation symmetry makes the twist the floor, that a field strength aligned with the twist's spin does, and that alignment together with the curvature term singling the twist out does (Section 7). A model of the edge as $c_1/t + c_2/t^2$ failed both of its pre-registered predictions. The conjecture that the all-sector edge equals $\min(x_{12}^*, 0)$ fails at and near $t = 2$ and is kept only for $t \geq 3$. The statement that the edge is the largest real root of P_2 is false: P_2 has further real roots where a higher eigenvalue of the competitor meets the twist. Six further tests were pre-registered (Section 8). At held-out points the edge clause failed at 4 of 38 points, where other blocks reach the twist first. At random circle-symmetric fields the reading that the competitor is nearly blind to x failed at 129 of 193 points. In an $SU(3)$ family with a free fibre field the twist is the floor of all nine tested sectors at no x of the 0.25 scan, at any of the 20 shapes, so the behaviour found here does not carry over to that family. In a fourth test, the same group stretched along the twist's own charge circle, she is the floor at 19 of 20 shapes, in one interval, on the predicted side; the competitor is again not blind. In a fifth, for $x > 0$, the floor of every sector is held by a state whose internal turning opposes the field along the circle, the state e_- of Theorem 5.1, at all 60 scored points. In a sixth, sweeping the stretched circle across the Weyl chambers of $SU(4)$ and $Sp(2)$, she lives on the coroot of her own highest root and just inside it, not on the principal circle and not on every regular circle.

BY ENOUGH, BUT NOT TOO MUCH. The field along the long circle must turn against the twist by enough that the discount $2xj/\sqrt{t}$ carries her below her competitors in the higher sectors, but not by so much that a state of the sector 0 undercuts her. In every grid of the family computed here ($t \leq 8$, $y \leq 3$), and at all 48 held-out points of Test A, the state that undercuts her from below is the lowest state of the sector-0 block of charge ± 1, which gives the lower end x_{lo} (computed; Proposition 5.4 turns this block into a proved bound for $H + GG^*$). The gauge-orthogonal state $\hat{\theta}^0 \otimes \tau_0$ gives a cruder bound, $x \geq r_{\mathrm{lo}}$, proved for both spectra. At random circle-symmetric fields (Test B) the sector-0 block sets the lower end at 110 of 193 points, blocks of the sectors 1 to 3 at 82, and the sector-0 block of charge 0 at one.

The thresholds t^* and t_A of [6] are therefore not special to the Berger field. They are where the Berger path meets the edge. The literature I checked (the chromomagnetic instability [20, 22],

homogeneous backgrounds on the round S^3 [2, 12]) did not contain such an edge; the nearest is the negative modes of covariantly constant backgrounds on the round sphere [2].

How the work was done. I did this work inside the GIGI repository, `https://github.com/nurdymuny/gigi`, as part of a data-first programme: fix in advance what would count as success and what as failure, then compute, and keep every output as a receipt (the strategy note `docs/research/yang-mills-strategy-2026-11-19.md`). The Berger field, where the twist was first found, is the background on which my two-ring lattice force [7] was tested [6]. The spectra in this paper are computed by standalone Python scripts in that repository, not by GIGI engine verbs; the repository holds the scripts, receipts and pre-registrations. Section 10 lists, claim by claim, the script, the receipt and the status.

Section 2 sets up the operator, the family, the Weitzenböck identity and the charge blocks. Section 3 gives the twist's eigenvalue and its anatomy. Section 4 derives the edge, its polynomial, the Berger crossings and the Lean check. Section 5 proves that the region is bounded on both sides and that $x > 0$ loses for $H + GG^*$. Section 6 proves the floor on a domain. Section 7 reports what decides the edge and what does not. Section 8 reports the pre-registered tests, Section 9 the scope and open problems, and Section 10 the data and receipts. Appendix A holds the charge-block rows and competitor polynomials, Appendix B the certificate details, and Appendix C the pre-registration details.

2 Setting: the operator, the circle-symmetric family, charge blocks

2.1 Conventions

The conventions are those of [6], stated compactly, with one correction: the bracket of the gauge algebra. $S^3 = SU(2)$ carries the left-invariant frame e_0, e_1, e_2 with $[e_a, e_b] = 2\epsilon_{abc}e_c$. The Berger metric $(t, 1, 1)$ is diagonal in it, with e_0 the long axis; the parameter $t > 0$ is *the stretch*, and the orbits of e_0 are *the long circle* (the fibre). $\hat{\theta}^i$ is the orthonormal coframe. A field is $A = \sum_i M_i \hat{\theta}^i$ with M_i constant in $\mathfrak{su}(2)$. The Lie algebra $\mathfrak{su}(2)$ has the basis τ_0, τ_1, τ_2 with

$$[\tau_a, \tau_b] = \epsilon_{abc}\tau_c,$$

the cross product on $\mathbb{R}^3$, so τ_a corresponds to $e_a/2$ and $\mathrm{ad}\, M_i$ acts on Lie components as $m_i \times \cdot$; τ_0 is along the long axis. (The Floor paper [6] says that τ_a has "the same brackets" as the frame; every formula there and here, and all of the code, uses the cross product.) The curvature is $F_{ij} = [M_i, M_j] - \sum_k c_{ij}^k M_k$.

The second variation is $Q(b) = \sum_{i<j} \|D_{ij}b\|^2 + 2\langle F_{ij}, [b_i, b_j]\rangle$, and H is its operator against the L^2 mass $\sum_i \|b_i\|^2$. The gauge map is $G\xi = (\hat{e}_i\xi + [M_i, \xi])_i$. The fields studied are in general not Yang–Mills critical points, so gauge directions are not zero modes; the *gauge-orthogonal spectrum* is the spectrum of PHP on $\ker G^*$. In the Peter–Weyl sector $j \geq 0$ (spin $j/2$), $b_i \in V_j \otimes \mathfrak{su}(2)$ and H is a $9(j+1)\times 9(j+1)$ Hermitian matrix. The frame fields act on V_j by ρ_0, ρ_1, ρ_2, with $[\rho_a, \rho_b] = 2\epsilon_{abc}\rho_c$ and $\rho_a^* = -\rho_a$; $J_z = (i/2)\rho_0$ and $J_\pm = (i/2)(\rho_1 \pm i\rho_2)$ form a standard angular-momentum triple. (The code's `spin_rep` labels the same triple with a cyclic relabelling of the axes, a unitary equivalence that changes no spectrum.)

The *floor* of a sector is its lowest gauge-orthogonal eigenvalue, or, where stated, its lowest eigenvalue of $H + GG^*$. Every statement below says which. The *edge* is the level-crossing locus where the twist's eigenvalue meets the lowest eigenvalue of another charge block, *the competitor*.

2.2 The circle-symmetric family

The family is

$$M_0 = x\,\tau_0, \qquad M_1 = y\,\tau_1, \qquad M_2 = y\,\tau_2,$$

a strength x along the long circle and a strength y across it. Three members recur. The Berger field is $x = (2-t)/\sqrt{t}$, $y = \sqrt{t}$ (proved to be the Levi-Civita field in Lemma 2.2); I call the curve it traces *the Berger path*. The multiples $A = s\theta$ of the Maurer–Cartan form are $x = 2s/\sqrt{t}$, $y = 2s$. The squashed meron lies in the family too, at $x > 0$ (its coordinates are computed numerically). The field strength of a member is

$$F_{12} = B\,\tau_0, \quad B = y^2 - 2\sqrt{t}\,x, \qquad F_{01} = (xy - 2y/\sqrt{t})\,\tau_2, \quad F_{02} = -(xy - 2y/\sqrt{t})\,\tau_1, \qquad (1)$$

so B is the field along the fibre and F_{01}, F_{02}, of size $|y(x-2/\sqrt{t})|$, lie across it. On the Berger path $B = 3t - 4$; on $A = s\theta$, $B = 4s(s-1)$, which vanishes at $s = 1$ as it must (`scripts/ricci_su2_twist_anatomy.py`, receipt `twist_anatomy.json`; (1) is also checked in `weitzenbock_family.json`).

Proposition 2.1 (Generality up to constant gauge)**.** *Let $A = \sum_i M_i \hat{\theta}^i$ be a left-invariant $SU(2)$ field on $(t, 1, 1)$ that is invariant under the right circle generated by e_0, lifted by a constant gauge circle of weight k about a Lie axis. Then A is constant-gauge-equivalent to a member of the family with $y \geq 0$. At $y = 0$ the members $(x, 0)$ and $(-x, 0)$ are gauge-equivalent.*

Proof. Write $M = (M_{ia})$ (frame i, Lie a) and take the gauge axis to be τ_0. The infinitesimal condition is $LM - kML = 0$, with L the $\mathfrak{so}(2)$ generator on the indices $1, 2$. Its solution space (the commutant), found symbolically, has dimension 1, 3, 3, 3, 1 for $k = -2, \ldots, 2$. For $k = \pm 2$ it is $m_0 = x\,\tau_0$, $m_1 = m_2 = 0$. For $k = 0$ it is m_0 arbitrary, $m_1 = m_2 = 0$. For $k = +1$ it is $m_0 = x\tau_0$, $m_1 = y\tau_1 - z\tau_2$, $m_2 = z\tau_1 + y\tau_2$, and for $k = -1$ it is $m_0 = x\tau_0$, $m_1 = -y\tau_1 + z\tau_2$, $m_2 = z\tau_1 + y\tau_2$. For $|k| \geq 3$ and for half-integer k only the weight-0 solution with $y = 0$ remains. Constant gauge rotations reduce each case. For $k = +1$, the rotation by $\arg(y + iz)$ about τ_0 maps (x, y, z) to $(x, \sqrt{y^2 + z^2}, 0)$. For $k = -1$, the pair (m_1, m_2) has Lie part $\left(\begin{smallmatrix} -y & z \\ z & y \end{smallmatrix}\right)$ on (τ_1, τ_2), a scaled reflection; the rotation by $\arg(y + iz)$ about τ_0 turns it into $\mathrm{diag}(-\rho, \rho)$ with $\rho = \sqrt{y^2 + z^2}$, and then the rotation by π about τ_2 ($\tau_0 \mapsto -\tau_0$, $\tau_1 \mapsto -\tau_1$) maps it to the family member $(-x, \rho)$. For $k = 0$, a rotation maps m_0 to $|m_0|\tau_0$, a member with $y = 0$; a rotation by π about τ_1 shows $(x, 0) \sim (-x, 0)$. The gauge maps were checked on the fields to 2.2×10^{-16} (`scripts/edge_wp4_design_checks.py`, receipt `research/edge-theorem-20261121/wp4_design_checks.json`); that receipt checks the case $k = -1$ only at $z = 0$, with the opposite sign convention $y \mapsto -y$, for which the rotation about τ_1 does the same job. □

The proposition says nothing outside its class. It does not cover fields that are circle-invariant but not left-invariant, lifts by non-constant gauge transformations, or circles other than the right circle about e_0. For $t \neq 1$ it assumes, without re-proving it, that the isometry group is $SU(2)_L \times U(1)_R$. As a code control (computed), full spectra of $H + GG^*$ in the sectors $j \leq 4$ at six random points agree after removing z to 1.95×10^{-15}, after the $k = -1$ reduction to $x \mapsto -x$ exactly (0.0), and after a random constant gauge frame to 2.23×10^{-15}. At $y = 0$ the spectrum is therefore even in x.

2.3 The Weitzenböck identity and the charge blocks

Lemma 2.2 (Weitzenböck identity for the family; proved)**.** *For all real x, y and $t > 0$,*

$$H + GG^* = \sum_i X_i^* X_i + R_0, \qquad X_i = \rho_i/\sqrt{g_i} + \Omega_i, \qquad R_0 = \mathrm{Ric} \otimes I - 2[F, \cdot\,], \tag{2}$$

as an identity in $U(\mathfrak{su}(2)) \otimes \mathrm{Mat}_9$, hence in every sector. Here $g = (t, 1, 1)$, $\Omega_i = I \otimes \mathrm{ad}\, M_i - \Gamma_i \otimes I$ with Γ_i the Levi-Civita connection matrix of the frame, $([F, \cdot\,]b)_i = \sum_k [F_{ik}, b_k]$, and $\mathrm{Ric} = \mathrm{diag}(2t, 4-2t, 4-2t)$ is the Ricci tensor of $(t, 1, 1)$. The Levi-Civita field is the member $x = (2-t)/\sqrt{t}$, $y = \sqrt{t}$, and F is given by (1)*.*

Proof. Exact symbolic computation in $U(\mathfrak{su}(2))$ with x, y real and $t > 0$ symbolic. The script builds H and G from Q, normal-orders every product in the Poincaré–Birkhoff–Witt basis, and finds that every non-constant word of $H + GG^* - \sum_i X_i^* X_i$ cancels and that the constant part minus $(\mathrm{Ric} \otimes I - 2[F, \cdot\,])$ is the zero matrix. The Ricci tensor is computed from the Koszul formula, each Γ_i is antisymmetric, and F matches (1). The same identity holds for an arbitrary constant M (nine free symbols) at the metric $(t, 1, 1)$. Two mutation tests (a wrong generator bracket, a wrong Ricci tensor) make the checks fail (`scripts/ricci_su2_weitzenbock_family_symbolic.py`, receipt `research/edge-theorem-20261122-proofs/weitzenbock_family.json`, 21.7 s). This is the Bochner–Weitzenböck formula of [5] (an accessible statement is [9]), with its signs and factors fixed for the conventions here. □

The lemma uses three standard facts, which are not re-proved: on V_j the triple (J_x, J_y, J_z) above has the usual matrix elements on $|l, m\rangle$, $l = j/2$ (Peter–Weyl); H is the operator of Q, the second variation of $E = \frac{1}{2}\sum_{i<k} \|F_{ik}\|^2$, from $F(A + b) = F + Db + [b_i, b_k]$; and $\rho_a^* = -\rho_a$ in L^2 (the right-regular representation of a unimodular group is unitary).

On V_j take the weights $m \in \{-l, \ldots, l\}$, $l = j/2$, along the long axis. Write the frame index and the Lie index in the eigenbasis of the rotation, with charges $c_f, c_l \in \{-1, 0, 1\}$.

Lemma 2.3 (Charge blocks; proved)**.** *For every member of the family, the charge $q = m + c_f + c_l$ is conserved by $H + GG^*$. Each sector is the orthogonal sum of charge blocks $B_{j,q}$, spanned by the at most nine states (m, c_f, c_l) with $m = q - c_f - c_l$, $|m| \le l$. An antiunitary map commutes with $H + GG^*$ and reverses q, so the blocks $B_{j,q}$ and $B_{j,-q}$ have the same spectrum. For a state (m, a), $a = (c_f, c_l)$, the diagonal entry is*

$$D(m, a) = \Big(w_a - \frac{2m}{\sqrt{t}}\Big)^2 + 4\big(l(l+1) - m^2\big) + C_{aa}, \qquad C = -(\Omega_1^2 + \Omega_2^2) + R_0, \tag{3}$$

with $w_a = c_f(t-2)/\sqrt{t} - c_l\, x$, and the ladder couplings are $2i\sqrt{(l-m)(l+m+1)}\,(\Omega_-)_{a'a}$ to $m+1$ and $2i\sqrt{(l+m)(l-m+1)}\,(\Omega_+)_{a'a}$ to $m-1$, with $\Omega_\pm$ the charge-basis parts of $\Omega_1 \pm i\Omega_2$.

Proof. In the charge basis Ω_0 is diagonal, $i\,\mathrm{diag}(w)$ with w real; Ω_+ raises the combined charge $c = c_f + c_l$ by 1 and Ω_- lowers it by 1; $\Omega_- = -\Omega_+^H$; C is Hermitian and preserves c. Each of these is an exact identity, and so is the block-operator identity

$$U^H(H + GG^*)U = \big(W - 2J_z/\sqrt{t}\big)^2 + 2(J_+J_- + J_-J_+) + C + 2i\,(J_+\Omega_- + J_-\Omega_+)$$

in $U(\mathfrak{su}(2)) \otimes \mathrm{Mat}_9$ after normal ordering, with $W = \mathrm{diag}(w)$ (receipt `weitzenbock_family.json`, part 2). Since J_z is diagonal and $J_\pm$ shift m by ± 1, each term preserves q, and with the standard matrix elements of $J_\pm$ the identity is entry for entry (3) and the ladder couplings. For the mirror, take $J \otimes K$, with J the real (j even) or quaternionic (j odd) structure of V_j and K complex conjugation on the frame and Lie indices. This is the argument of [6, Lemma "Charge blocks"] with x and y free. □

The table of w_a, the moduli of the entries of C and $\Omega_\pm$, and the exact sector-0 blocks are in Appendix A. Every entry of C has degree at most one in x, and the ladder couplings $\Omega_\pm$ do not involve x. The blocks are real symmetric, and the twist row is alone in a 1×1 block: $D(l,(1,1)) - \lambda = 0$ and its mirror $D(-l,(-1,-1)) - \lambda = 0$ identically in l, x, y, t (`weitzenbock_family.json`, `gershgorin_lemma.json`).

2.4 What is proved, and the transcription condition (T)

Lemmas 2.2 and 2.3 prove that the closed-form rows are the charge blocks of $H + GG^*$. The certificates of Sections 5 and 6, and the edge polynomials of Section 4, do not read those proved rows directly. They evaluate their own code: the function `symbolic_rows` of `scripts/ricci_su2_exact_edge.py` (used by the edge functions, the edge polynomials, the competitor map, `ricci_su2_family_large_j.py` and the bulk step of `edge_wp2_interval_proof.py`), the scaled near-end matrices of `edge_wp2_interval_proof.py`, the construction in `ricci_su2_family_block_cert.py`, and the exact blocks of `edge_wp3_slice_iff.py`. Most of that link is now proved: an exact check (`scripts/ricci_su2_rows_transcription_check.py`, receipt `research/edge-theorem-20261122-proofs/rows_transcription.json`) shows, by sympy equality of the symbolic expressions themselves, that the rows of `symbolic_rows`, the rows of the domain certificate (with $L_\pm = 2i\Omega_\pm$ and $t = s^2$), the rebuilt rows of `edge_wp1_block_polynomials.py` and `edge_wp3_slice_iff.py`, and the edge polynomial's block $B_{4,0} - \lambda_4$ are exactly the rows of Lemma 2.3. What remains I state once:

(T) *The scaled near-end matrices of `edge_wp2_interval_proof.py`, and the slice construction of `edge_wp3_slice_iff.py` built on its (proved) rows, equal the corresponding objects of Lemma 2.3.*

(T) is checked numerically: the near-end matrices against the blocks to 4.5×10^{-16}, and the exact slice blocks against them to 2.8×10^{-14}. Independently, the blocks agree with full sector spectra from the general builder, built from Q with no charge blocks, at 12 random points to 1.47×10^{-15} (`research/su2-floor-family-20261119/exact_edge.json`). Results whose proof runs through (T) are labelled PROVED under (T). Results proved directly from Q, from Lemmas 2.2 and 2.3, or through code whose rows are proved equal to them, are labelled PROVED.

3 The twist and its closed form

Proposition 3.1 (The twist is exact; PROVED)**.** *At every member of the family and in every sector j, the twist $b = f\,(\hat\theta^1 + i\hat\theta^2) \otimes (\tau_1 + i\tau_2)$ is an eigenvector of $H + GG^*$ and of H, and it is gauge-orthogonal. Its eigenvalue has multiplicity at least two in the full spectrum, shared with its mirror.*

Proof. In charge coordinates b is $(m, c_f, c_l) = (l, 1, 1)$, of charge $q = l + 2$. It is the unique state of maximal charge, so it spans a 1×1 block and is an eigenvector of $H + GG^*$ (Lemma 2.3). A

gauge parameter ξ carries only a weight and a Lie index, so the charges in the range of G reach at most $l+1$. Hence $G^*b = 0$ and $Hb = (H + GG^*)b$. By Lemma 2.3, the block of charge $-l-2$ has the same entry. This is the counting of [6] with x and y free. □

In the computations the multiplicity is exactly two where checked: in the sectors $j \le 4$ at $(x, y, t) = (-2, 1.5, 4)$ and $(-1, 0.7, 6)$, in both the full and the gauge-orthogonal spectra. Over $x \in [-40, 1]$, $t \in \{3, 5, 10\}$, $y \in \{0.5, 1.5, 3\}$, $j \le 12$, the mirror copy is present: the mirror's value minus λ is at least -6.8×10^{-13} (double precision). A single-copy removal of the twist is therefore an error; every edge computation removes two copies.

Proposition 3.2 (The closed form; proved)**.** *For every $t > 0$, $x, y \in \mathbb{R}$ and $j \ge 0$, the twist's eigenvalue is*

$$\lambda(x, y, t, j) = \left(x + \frac{j+2}{\sqrt{t}}\right)^2 + 2\sqrt{t}\, x - y^2. \tag{4}$$

On the Berger field it equals $\lambda_t(j)$ exactly. On $A = s\theta$ it equals $(j + 2s + 2)^2/t + 4s(1 - s)$.

Proof. The twist is alone in its charge block, so its eigenvalue is its diagonal entry (3) at $m = l$, $a = (1, 1)$, with $w = \sqrt{t} - x - 2/\sqrt{t}$ and $C = 4\sqrt{t}\, x - t - y^2 + 4$. Then $(w - j/\sqrt{t})^2 = (x + (j+2)/\sqrt{t})^2 - 2\sqrt{t}\, x - 2(j+2) + t$, the second term of (3) is $4l = 2j$, and the sum is (4); the receipt of Lemma 2.2 checks $D(l, (1, 1)) - \lambda = 0$ identically. Substituting $x = (2 - t)/\sqrt{t}$, $y = \sqrt{t}$ gives $\lambda_t(j)$ with difference 0, and substituting $x = 2s/\sqrt{t}$, $y = 2s$ gives the second formula (`scripts/ricci_su2_twist_family_closed_form.py`, receipt `research/su2-floor-family-20261119/twist_family_closed_form.txt`). As a check (computed), it agrees with the general builder at 40 random (x, y, t, j) to 1.4×10^{-15}; and directly from Q, for $j = 0, \ldots, 6$, the twist vector is an exact eigenvector with eigenvalue λ_j (`direct_rayleigh.json`). □

Corollary 3.3 (The lift and its discount)**.** *The cost of lifting the twist from the sector 0 to the sector j is*

$$\lambda(j) - \lambda(0) = \frac{j^2 + 4j}{t} + \frac{2xj}{\sqrt{t}}.$$

For $j \ge 1$ the second term lowers the cost if and only if $x < 0$, that is, when the field along the long circle turns against the twist's own rotation.

Proof. Expand (4): $(x + (j+2)/\sqrt{t})^2 - (x + 2/\sqrt{t})^2 = 2xj/\sqrt{t} + ((j+2)^2 - 4)/t$. □

On the Berger field $x = (2 - t)/\sqrt{t}$, which changes sign at $t = 2$. That is the stretch at which, by the Casimir remark of [6], the coupling of the lift to the stretch vanishes: $\lambda_2(j) - \lambda_2(0) = (j^2 + 4j)/2$, and $\lambda_2(0) = 0$. For $t > 2$ the Berger field lies on the side $x < 0$, where the discount helps the twist. Figure 1 shows both halves of the picture. In panel (a), see how the twist gathers into a cap about the pole of the long circle as the sector rises; in panel (b), see that the lift term is a discount exactly on the shaded side $x < 0$, and a steeper one for smaller stretch.

Proposition 3.4 (Anatomy; proved)**.** *Let $\beta = (\hat{\theta}^1 + i\hat{\theta}^2) \otimes (\tau_1 + i\tau_2)$ be the twist's internal frame. For every x, y, t and j:*

1. *$X_0 b = i\kappa\, b$ with $\kappa = (t - 2)/\sqrt{t} - x - j/\sqrt{t}$. The three terms are the Levi-Civita rotation of the frame, the gauge field acting on the twist's Lie charge (minimal coupling), and the orbital motion along the fibre.*

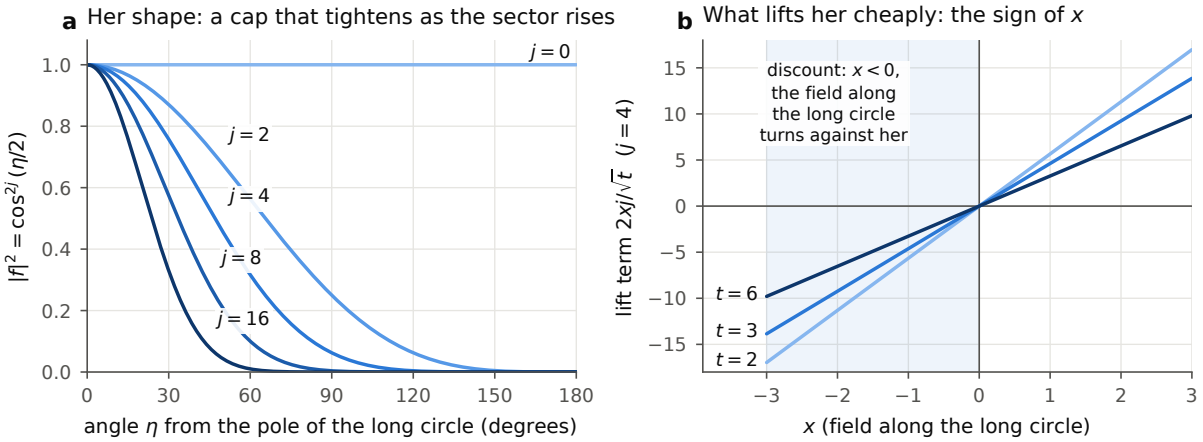

FIGURE 1. Helike's shape and lift. (a) Her amplitude on the base sphere, $|f|^2 = \cos^{2j}(\eta/2)$, against the angle η from the pole of the long circle, for $j = 0, 2, 4, 8, 16$. She gathers into a cap about the pole as the sector rises. (b) The lift term $2xj/\sqrt{t}$ of Corollary 3.3 at $j = 4$, for $t = 2, 3, 6$. It is negative, a discount, exactly when $x < 0$ (shaded), that is, when the field along the long circle turns against her rotation. Both panels plot closed forms (the top weight of V_j, and Corollary 3.3); nothing in them is fitted.

2. $(\Omega_1 + i\Omega_2)\beta = 0$, *so with the top weight* $X_+ b = 0$*: the twist is a lowest Landau level across the whole family.*
3. $R_0\beta = (\mathrm{Ric}_\perp - 2B)\beta$ *with* $\mathrm{Ric}_\perp = 4 - 2t$ *and* B *as in* (1)*; the part* $-2[F, \cdot\,]$ *contributes* $4\sqrt{t}\,x - 2y^2 = -2B$.
4. $\lambda = \kappa^2 + (2j + t + y^2) + (\mathrm{Ric}_\perp - 2B)$*: fibre momentum squared, the transverse lowest-Landau-level term, and the curvature term (Ricci across the fibre, and spin against the fibre field).*
5. $\partial\lambda/\partial x = -2\kappa + 4\sqrt{t}$*. The strength* x *enters twice: through* κ *by minimal coupling, and through* B *by the spin.*
6. *On the Berger path the gauge part of* κ *equals the frame part, and* $\kappa = (2t - 4 - j)/\sqrt{t}$*, the transverse term is* $2(j + t)$*, the curvature term is* $12 - 8t$*, and* $B = 3t - 4$.

Proof. Exact symbolic computation of each identity; the parts in (4) minus (4) is 0 (script `scripts/ricci_su2_twist_anatomy.py`; receipt `twist_anatomy.json` in `research/su2-floor-family-20261119/`). Item (5) is the derivative of (4): $-2\kappa + 4\sqrt{t} = 2(x + (j+2)/\sqrt{t}) + 2\sqrt{t}$. Item (6) recovers the proposition of [6] that the twist is a lowest Landau level on the Berger field. The algebraic identity of item (4), with κ and B given by their formulas, and the values $\kappa = (2t - 4 - j)/\sqrt{t}$, $B = 3t - 4$ and $\lambda = \lambda_t(j)$ on the Berger path, are also proved in Lean 4 (`price_anatomy`, `kappa_berger`, `fieldCurv_berger`, `price_berger`; Section 4.6). □

Near the edge the twist's slope in x is about 10 at every point computed (9.74, 9.62, 10.18 at the three points of Section 4.2; computed).

Remark 3.5 (A reading). The structure of Proposition 3.4 resembles a lowest-Landau-level kinetic term plus a Zeeman term with gyromagnetic factor 2. That is the flat-space mechanism of the unstable mode of Nielsen and Olesen [20], stated explicitly in [4]. Landau levels on spheres are a

Table 1. The edge in the sectors $j \le 12$, x_A^* / x_S^* (double precision; not certified). For $y \ge 1.5$ and $y = \sqrt{t}$ the competitor is $B_{4,0}$ throughout. Every positive entry is an artefact of the cut-off $j \le 12$: for x_A^* this is proved (Theorem 5.1); for x_S^* it is supported by computation (Section 5). The row $t = 2$ is not the all-sector edge at $y = 0.5$ either (Section 5.5). Receipt `research/su2-floor-family-20261119/exact_edge.json`.

t	$y = 0.5$	$y = 1.5$	$y = \sqrt{t}$
2	−0.613240 / −0.605292	−0.682793 / −0.657567	−0.677814 / −0.655100
3	−0.335488 / −0.318061	−0.371582 / −0.351580	−0.382168 / −0.355187
4	−0.202972 / −0.191702	−0.208048 / −0.191652	−0.221163 / −0.189150
6	−0.082842 / −0.078032	−0.044874 / −0.033249	−0.035386 / +0.008031
8	−0.033799 / −0.031530	+0.031482 / +0.040169	+0.082513 / +0.138269

standard construction [8, 28]. I note the resemblance only; no limit relating the two is proved, and none of these sources says anything about Berger spheres.

Remark 3.6 (The split of R_0). The split $R_0 = \mathrm{Ric} \otimes I - 2[F, \cdot\,]$ is now part of Lemma 2.2, exactly, for the whole family. (Earlier it was checked numerically to 4×10^{-15} on the Berger field and the squashed meron at $t = 1, 2, 3, 4, 6, 8$.) On the twist's internal frame the Ricci share is $4 - 2t$. The field-strength share is $-2B$, which is $8 - 6t$ on the Berger field (-4 at $t = 2$, -40 at $t = 8$), but positive on the squashed meron: $+1.2614$ at $t = 2$, $+0.9265$ at $t = 3$, $+0.7334$ at $t = 4$, $+0.5183$ at $t = 6$, $+0.4010$ at $t = 8$ (computed, because the meron's coordinates are; `research/su2-floor-family-20261119/gyromagnetic_split.txt`). Read through item (3) of Proposition 3.4, on the squashed meron the field strength is opposed to the twist's spin. Section 7 shows that this alone does not decide the floor.

4 The edge

4.1 Edge functions

By Lemma 2.3, whether the twist is the lowest eigenvalue of $H + GG^*$ in the sectors $j \le J$ is a comparison between λ and the lowest eigenvalues of finitely many blocks. Define

$$\phi_A(x) = \min_{j \le J} \min_{q \ne \pm(l+2)} \left[\lambda_{\min}(B_{j,q}) - \lambda_j\right],$$

with both twist blocks excluded, and for the gauge-orthogonal spectrum $\phi_S(x) = \min_{j \le J}[\mu_{\min,j} - \lambda_j]$, where μ is the slice spectrum from the general builder after removing two copies of λ_j. The edge x_A^* (resp. x_S^*) is the largest x in the scan window where ϕ changes sign from ≥ 0 to < 0, located by Brent's method to 10^{-12}; x_{12}^* denotes the $H + GG^*$ edge with $J = 12$. At the edge λ_j is an eigenvalue of the competitor block, so the edge is a root of $\det(B_{j,q}(x, y, t) - \lambda_j) = 0$. The gauge-orthogonal edge is slightly higher than the $H + GG^*$ edge at every point of Table 1: at $t = 3$ by 0.027 ($y = \sqrt{3}$) and 0.020 ($y = 3/2$). In double precision the gauge-orthogonal edges agree with the independent bisection of the earlier edge test at its 21 points to 3×10^{-5}, within that bisection's tolerance 10^{-4} (`scripts/ricci_su2_exact_edge.py`, receipt `exact_edge.json`).

Table 1 gives the edge at five stretches. At $t = 2$ and $y = 0.5$ the competitor is $B_{3,1/2}$; at $t = 3$, $y = 0.5$ it is $B_{2,-1}$, the mirror of $B_{2,1}$. Within $j \le 12$ the edge rises with the stretch and turns

positive for strongly stretched spheres with a strong cross field. That is an artefact of the cut-off: Section 5 proves that for $x > 0$ high sectors undercut the twist in $H + GG^*$, and the computations there support the same for the gauge-orthogonal spectrum.

4.2 The competitor

For a cross field y around 1 and above, and moderate stretch, the edge is set by $B_{4,0}$, the 9×9 charge-0 block of the sector $j = 4$, with entries in $\mathbb{Q}(\sqrt{2}, \sqrt{3})$. (In the map of Section 4.5, for $t \le 6$ its region runs from $y \approx 0.75$–0.99 up to a curve from $y \approx 1.9$ at $t = 2$ to $y \approx 3$ at $t \approx 5.7$.) At the three points computed, its lowest state is a mirror-symmetric superposition dominated by $(m, c_f, c_l) = (+2, -1, -1)$ and $(-2, +1, +1)$: orbit and internal spin opposed, total fibre charge zero. The twist is charged, with orbit and spin aligned. At these three points the competitor is nearly blind to x. In double precision:

point (x, y, t)	weight in $m = \pm 2$	competitor slope	twist slope ($j = 4$)
Berger at t^*: $(-0.42496,\ 1.64257,\ 2.69803)$	0.62	-1.561	9.741
$(-0.19,\ 2,\ 4)$	0.66	-0.623	9.620
$(0.14,\ \sqrt{8},\ 8)$	0.73	$+1.684$	10.179

This is a property of $B_{4,0}$, not of the edge in general. The pre-registered Test B (Section 8) measured the competitor's slope at 193 random fields, and at 129 of them it is at least half the twist's; the charged competitors, mostly $B_{1,\pm 3/2}$, are steep. The function $\lambda_{\min}(B_{4,0}) - \lambda(x, y, t, 4)$ has negative first differences on a 241-point grid of $x \in [-3, 3]$ at all 47 distinct pairs (t, y) tested, t from 2 to 10 and y from 0.5 to 3 (computed; receipt `twist_anatomy.json`). An operator-norm bound on $\partial_x B_{4,0}$ is not enough to prove monotonicity: it works at 21 of 27 edge points and fails at every point with $y = \sqrt{t}$, $t \ge 4$.

4.3 The edge polynomial

Proposition 4.1 (The edge polynomial; PROVED)**.** *Let $s = \sqrt{t}$ and $P(x, y, s) = \det\big(s^2(B_{4,0}(x, y, s^2) - \lambda(x, y, s^2, 4)\, I)\big)$. Then $P \in \mathbb{Z}[x, y, s]$ has 473 terms, degrees $(12, 14, 28)$ in (x, y, s) and total degree 32, and*

$$P = -16384\, P_1 P_2,$$

with P_1, P_2 irreducible over $\mathbb{Q}$, each of multiplicity one and each even in y. P_1 has degrees $(5, 6, 12)$ in (x, y, s) and 61 terms; P_2 has degrees $(7, 8, 16)$ and 113 terms. They begin

$$P_2 = -8s^{16}x^2 + 24s^{15}x^3 + 8s^{15}xy^2 - 4s^{14}x^4 - 42s^{14}x^2y^2 - 320s^{14}x^2 - 2s^{14}y^4 - 11s^{13}x^5 + \cdots,$$
$$P_1 = 2s^{12}x^2 - 5s^{11}x^3 - 3s^{11}xy^2 - 24s^{11}x - s^{10}x^4 + \cdots.$$

Proof. Exact symbolic determinant over $\mathbb{Q}(\sqrt{2} + \sqrt{3})[x, y, s]$ and exact factorization [24] (script `scripts/ricci_su2_edge_polynomial.py`; the full polynomials are in the receipts `edge_polynomial.txt` and `edge_polynomial.srepr` of `research/su2-floor-family-20261119/`). The content -16384 is recorded with this normalisation in the receipt `wp1_block_polynomials.json` of `research/edge-theorem-20261121/`. The factorization is also proved in Lean (Theorem `edgeDet_factor`, Section 4.6). A second builder of the blocks recovers the same edge factor exactly (quotient 1, remainder 0; `wp1_block_polynomials.txt`). Its full determinant was compared with `edge_polynomial.srepr` only by the ratio 1 at four rational points, which is a computed check, not a proof. □

P_2 vanishes on the numerically located edge wherever $B_{4,0}$ is the competitor: at all 77 grid edges of the map the nearest root of P_2 lies within 2.4×10^{-13} of the edge, while the scale-free residual of P_1 there is at least 2.6×10^{-3}, and at the 76 grid edges where P_1 has a real root nearby, the nearest root of P_1 is 0.13–0.67 away, closest at $(t, y) = (2, 1.75)$ (computed; receipt `wp1_poly_check_final.json`). *The edge is not in general the largest real root of P_2.* On the 18 known-answer rows of Table 1's receipt with $y = 1.5$ or $y = \sqrt{t}$, P_2 has three or four further real roots in $[-3, 3]$ above the edge, from about 0.55 ($t = 2$) to 3.5 ($t = 12$, $y = \sqrt{t}$), where a higher eigenvalue of $B_{4,0}$ meets λ_4. The edge is the root at which the *lowest* eigenvalue of $B_{4,0}$ equals λ_4. This was found by a known-answer gate of a pre-registered test, before any of its held-out points was computed (Section 8); the earlier statement "largest real root" is withdrawn.

4.4 The Berger crossings

Proposition 4.2 (Berger restriction; PROVED)**.** *For $s \neq 0$,*

$$P_2\Big(\frac{2 - s^2}{s}, s, s\Big) = -32\,(s - 1)(s + 1)\,Q_{16}(s),$$

$$Q_{16}(s) = 3s^{16} + 121s^{14} + 1066s^{12} - 2836s^{10} - 18624s^8 + 20992s^6 + 181248s^4 - 425984s^2 + 262144,$$

the polynomial of [6, Remark "Below the range"] whose largest positive root is $s = \sqrt{t_A}$, $t_A = 2.73112227823811362\ldots$. So t_A is algebraically a root of the edge polynomial on the Berger path.

Proof. Proved in Lean (`edgeFactor_berger`, by `field_simp` and `ring`), together with a root of Q_{16} in $[1.65261, 1.65262]$ and a zero of the restriction with $s^2 \in [2.73111, 2.73116]$. The script `scripts/ricci_su2_edge_polynomial.py` checks only that Q_{16} divides the restriction (receipt `edge_polynomial.txt`). □

Along the Berger path $x = (2 - t)/\sqrt{t}$, $y = \sqrt{t}$, the computed edges are crossed as follows (double precision, root-finding to 10^{-12} on exact ingredients; receipt `exact_edge.json`). The $H + GG^*$ edge is crossed at $t = 2.7311222782381144$, within 8×10^{-16} of t_A. The gauge-orthogonal edge is crossed at $t = 2.6980269405211303$, which agrees with $t^* \approx 2.698026940520$ (the double-precision bisection of the Floor paper) to about 10^{-12}, the precision of both computations. Both crossings go through the sector $j = 4$, the first through the block $B_{4,0}$. That t_A is a root of P_2 on the path is proved (Proposition 4.2); that the path crosses the edge there is computed. Between t^* and t_A the eigenvalue of $H + GG^*$ below $\lambda_t(4)$ is not gauge-orthogonal (computed; [6, Remark "Below the range"]).

Figure 2 shows the two crossings. In panel (a), see the twist's eigenvalue (blue) fall through the lowest gauge-orthogonal competitor at t^* and through the lowest $H + GG^*$ competitor at t_A; in panel (b), see the two margins cross zero at those two stretches, with their kinks further right, where they are already positive.

The thresholds of [6] are therefore where the Berger path meets the edge, not properties of the Berger field alone. The edge is a crossing, not an avoided one: the twist is alone in its charge block, every competitor found has a different charge, and eigenvalues of different symmetry type may cross where those of one type generically do not [27].

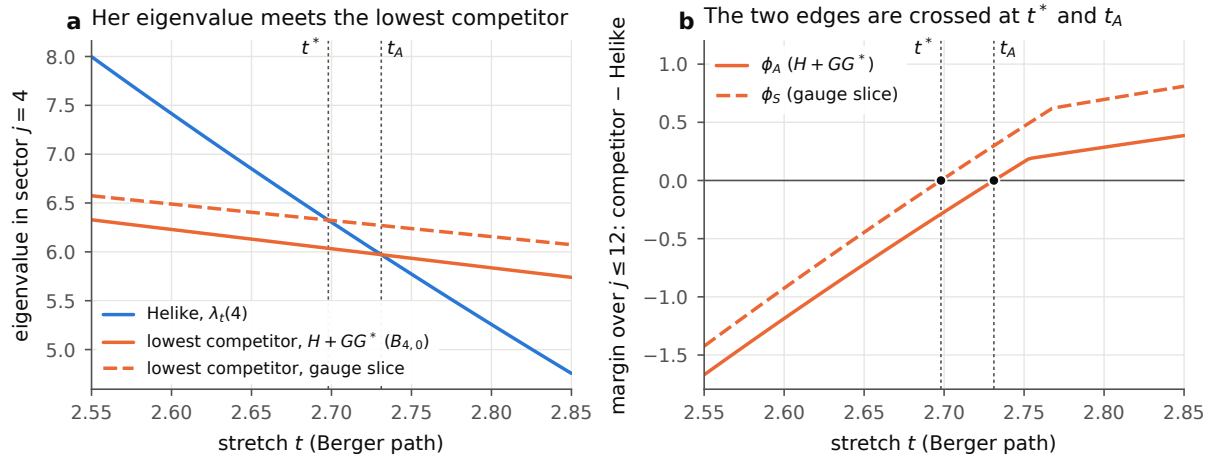

Figure 2. The Berger path meets the edge (computed, double precision; 121 values of t in $[2.55, 2.85]$). (a) In the sector $j = 4$: her eigenvalue $\lambda_t(4)$ (blue), the lowest other eigenvalue of $H + GG^*$ (solid; block $B_{4,0}$) and the lowest gauge-orthogonal eigenvalue after removing her two copies (dashed). (b) The margins over $j \le 12$: ϕ_A for $H + GG^*$ (solid) and ϕ_S for the gauge slice (dashed). The slice margin crosses zero at t^* (receipt value 2.6980269405211303) and the $H + GG^*$ margin at t_A (receipt value 2.7311222782381144, within 8×10^{-16} of the largest root of Q_{16}). Both crossings go through the sector 4. Between t^* and t_A the eigenvalue below $\lambda_t(4)$ is not gauge-orthogonal. The kinks near $t = 2.755$ ($H + GG^*$) and $t = 2.77$ (slice) are where the minimum over sectors passes to the block $(1, \pm 3/2)$, or to the sector 1. They lie above both crossings, where the margins are positive.

4.5 *Other competitors*

On a grid of 132 points, $t = 2, \ldots, 12$ by $y = 0.25, \ldots, 3$, with $j \le 12$ and the window $[-3, 1]$, eight blocks (up to the mirror $q \leftrightarrow -q$) set the $H + GG^*$ edge (computed). Their edge factors were derived exactly (Table 3 in Appendix A). All 132 grid edges are roots of the right factor, to 2.4×10^{-13} (computed). At every grid point ϕ_A has a single sign change on a 401-point scan of $[-3, 1]$, and $\phi_A(-3) \ge 1.43$.

The regimes are ordered by the cross field. At small y the competitor is $B_{2,1}$, up to $y \approx 0.57$–0.67; then $B_{3,1/2}$, up to $y \approx 0.75$–0.99; then $B_{4,0}$; and at large y and small t, $B_{1,3/2}$ (and $B_{2,2}$ at $t = 2$, $y \ge 2.75$). For $t \ge 7$ at $y \approx 0.75$–1 the blocks $B_{1,1/2}$ and $B_{1,3/2}$ compete. The colours of Figure 3 (Section 5) show these regimes at five stretches. Examples of switches and the closest runner-up gaps are in Appendix A. Six of the eight blocks belong to two near-top families of charge $q = l + 1$ and $q = l$; only $B_{4,0}$ and $B_{3,1/2}$ are sporadic. Those families govern the high sectors, and Section 5 uses them.

4.6 *Lean formalisation*

The algebraic identities above, and the closed form's anatomy as an algebraic identity, are proved in Lean 4 [17] (v4.36.0) with Mathlib [18]: sixteen theorems, with no `sorry` and no axioms beyond `propext`, `Classical.choice` and `Quot.sound` (on the branch `feat/helike-lean`: `docs/papers/berger-spectrum/lean/Helike/Edge.lean` and `Price.lean`). The four theorems of `Edge.lean` are the factorization `edgeDet` $= -16384\, P_1 P_2$, the Berger restriction, a root of Q_{16} in $[1.65261, 1.65262]$, and a crossing of $P_2 = 0$ by the Berger path with $s^2 \in [2.73111, 2.73116]$. The

twelve of `Price.lean` are listed in Appendix B.5.

What Lean does not check. Lean checks polynomial identities and the two brackets. It does not check that `edgeDet` is the determinant of $s^2(B_{4,0} - \lambda_4 I)$ (a computer-algebra step), that the root of P_2 is the edge (an eigenvalue comparison), that the twist is the floor anywhere, that `price` is an eigenvalue of the Hessian, or that the Lean `kappa` and `fieldCurv` are the fibre eigenvalue and field strength of Proposition 3.4 (1) and (3); in Lean they are formulas. Those rest on Lemmas 2.2 and 2.3, Propositions 3.1–4.1, and the certificates of Sections 5 and 6.

5 The region is bounded, and $x > 0$ loses

Section 4 locates the edge in the sectors $j \le 12$. Two facts change the picture once all sectors and all x are allowed. On the side of positive x the twist always loses in $H + GG^*$, to high sectors. On the side of very negative x it loses too, to states of the sector $j = 0$. Its region in x is therefore bounded on both sides.

Throughout, $l = j/2$, and a row of a charge block is labelled by its weight $m = l - \xi$ and its type $a = (c_f, c_l)$, as in Section 2. Write $\lambda_j = \lambda(x, y, t, j)$ for the twist's eigenvalue of Proposition 3.2.

5.1 Positive x

Theorem 5.1 (For $x > 0$ the twist is not the floor of $H + GG^*$ in every sector; proved)**.** *Let $t > 0$, $x, y \in \mathbb{R}$ and $l \in \frac{1}{2}\mathbb{Z}_{\ge 0}$.*

1. *In the charge block $B_{2l,l}$, the state e_- of weight $m = l$ and type $(1, -1)$ satisfies*
$$\langle e_-, (H + GG^*)e_- \rangle - \lambda_{2l} = -\frac{8lx}{\sqrt{t}} - 4\sqrt{t}\,x + 4y^2 - \frac{8x}{\sqrt{t}}.$$
2. *In the charge block $B_{2l,l+1}$, the state e_0 of weight $m = l$ and type $(1, 0)$ satisfies*
$$\langle e_0, (H + GG^*)e_0 \rangle - \lambda_{2l} = -\frac{4lx}{\sqrt{t}} - 2\sqrt{t}\,x - x^2 + 3y^2 - \frac{4x}{\sqrt{t}}.$$
3. *Consequently, if $x > 0$, the twist is not the lowest eigenvalue of $H + GG^*$ in the sector $j = 2l$ for every*
$$l > \frac{\sqrt{t}\,(4y^2 - 4\sqrt{t}\,x - 8x/\sqrt{t})}{8x}$$
(for every l if the right side is negative). In particular, for $x > 0$ the twist is not the lowest eigenvalue of $H + GG^*$ in every sector.

Proof. Items 1 and 2 are computed directly from Q, with no charge blocks. For $j = 0, \dots, 6$ the two Rayleigh quotients are exact symbolic expressions in x, y, t and equal the displayed formulas. $H + GG^*$ is quadratic in the ρ_a, and on the top vector $|l, l\rangle$ the moments $\langle J_z \rangle = l$, $\langle J_z^2 \rangle = l^2$, $\langle J_x^2 \rangle = \langle J_y^2 \rangle = l/2$ and the rest are polynomials in l of degree at most two. So both sides are polynomials of degree at most two in l, and agreement at seven values of l proves the identities for every l (`scripts/ricci_su2_direct_rayleigh.py`, receipt `research/edge-theorem-20261122-proofs/direct_rayleigh.json`). The same formulas also follow from the rows of Lemma 2.3 through the identity

$$D_{m,a} - \lambda_{2l} = 4\xi(2l - \xi)\Big(1 - \frac{1}{t}\Big) + l\,K_a + E_a(\xi) + R_a, \qquad K_a = 4 - \frac{8}{t} - \frac{4(w_a + x)}{\sqrt{t}}, \tag{5}$$

with $E_a(\xi)$ and R_a free of l, $K_{(1,1)} = 0$, $K_{(1,0)} = -4x/\sqrt{t}$ and $K_{(1,-1)} = -8x/\sqrt{t}$, verified symbolically for all nine types (script `scripts/edge_wp2_symbolic.py`; receipt `wp2_symbolic.txt` in `research/edge-theorem-20261121/`). Both states are unit vectors of charge l and $l+1$, while the twist has charge $l+2$, so they lie in blocks other than the twist's. A one-vector Rayleigh quotient bounds the lowest eigenvalue of a block above. For $x > 0$ the coefficient of l in item 1 is $-8x/\sqrt{t} < 0$, which gives item 3. As a check, the unmodified double-precision general builder reproduces both formulas at four points, among them -2.87748268961 at $(x, y, t, j) = (0.37, 1.3, 2.7, 6)$, to 5.7×10^{-14}. □

The theorem is stated for $H+GG^*$. The states e_- and e_0 are not gauge-orthogonal ($\|G^*e_-\|^2 = y^2$, exact), and projecting them onto $\ker G^*$ can raise the Rayleigh quotient, so for the gauge-orthogonal spectrum the conclusion is supported by the computations below but not proved.

Corollary 5.2. *Let $x^*_{12}(t, y)$ be the upper end of the set of x at which the twist is the lowest eigenvalue of $H + GG^*$ in every sector $j \le 12$ (Section 4; it is located numerically on grids). The set of x at which the twist is the lowest eigenvalue of $H + GG^*$ in every sector lies in $x \le \min(x^*_{12}, 0)$. In short, the all-sector edge of $H + GG^*$ is at most $\min(x^*_{12}, 0)$.*

Proof. The bound ≤ 0 is Theorem 5.1. The bound $\le x^*_{12}$ holds because the all-sector condition contains the condition in $j \le 12$. □

The positive edges of the cut-off (double precision; not certified). At all 58 grid points of the competitor map with $x^*_{12} > 0$, some sector $j > 12$ undercuts the twist in $H + GG^*$ at x^*_{12}; the minimising charge, where scanned, was $|q| = l + 1$ or l. In the other direction, at $x = -0.01$ and $x = -0.001$ at 57 of these points, nothing below the twist was found in the near-top blocks of $13 \le j \le 2000$ or in any block of $j \le 12$; the smallest margin is 0.029. For the gauge-orthogonal spectrum, an independent full-sector builder gives the margin -0.581 at $j = 120$ at $(x, y, t) = (0.1, \sqrt{10}, 10)$. The point $x = 0$ is degenerate: there $K_{(1,0)} = K_{(1,-1)} = 0$ and a proof would need a second-order argument. A worked example, the near-$x = 0$ margins and Table 7 are in Appendix B.4.

5.2 Very negative x

Proposition 5.3 (A gauge-orthogonal lower bound; proved)**.** *Let $v = \hat{\theta}^0 \otimes \tau_0$ in the sector $j = 0$ (weight $m = 0$, type $(0, 0)$, charge 0). For every (x, y, t) with $t > 0$:*

1. *$G^*v = -[M_0, \tau_0] = 0$, so v is gauge-orthogonal; it has charge 0, so it is orthogonal to both copies of the twist (charge ± 2 in the sector 0);*
2. *$\langle v, (H + GG^*)v\rangle = \langle v, Hv\rangle = 4t + 2y^2$, independent of x;*
3. *the twist is neither the lowest eigenvalue of $H + GG^*$ nor the lowest gauge-orthogonal eigenvalue in the sector $j = 0$ whenever $x < r_{\mathrm{lo}}$ or $x > r_{\mathrm{hi}}$, where*

$$r_{\mathrm{lo,hi}}(t, y) = -\left(\sqrt{t} + \frac{2}{\sqrt{t}}\right) \mp \sqrt{5t + 3y^2 + 4}$$

are the roots of $\lambda_0(x) = 4t + 2y^2$.

Proof. Items 1 and 2 are computed directly from Q in exact arithmetic (receipts `direct_rayleigh.json` and `lower_edge_closed_form.json`; the check $G^*v = 0$ is also in `wp4_design_checks.json`). By hand: R_0 gives $\mathrm{Ric}_{00} = 2t$, since $([F, v])_0 = 0$; the Lie parts of Ω_1 and Ω_2 give $\|[M_i, \tau_0]\|^2 = y^2$ each; the Levi-Civita parts give t each; the total is $4t + 2y^2$. Item 3: $\lambda_0(x)$ grows like x^2, while the Rayleigh quotient of v does not move. Where $\lambda_0 > 4t + 2y^2$, the vector v, orthogonal to the twist and its mirror and inside the gauge slice, has Rayleigh quotient below λ_0 for both $H + GG^*$ and the operator on the slice. Solving the quadratic $\lambda_0(x) = 4t + 2y^2$ gives $r_{\mathrm{lo,hi}}$. □

Examples: $r_{\mathrm{lo}}(3, 0.5) = -7.3308$, $r_{\mathrm{lo}}(3, 3) = -9.6691$, $r_{\mathrm{lo}}(10, 0.5) = -11.1941$ and $r_{\mathrm{lo}}(10, 3) = -12.7947$. Since r_{lo} decreases in y and, for $t > 2$, in t, it follows that $r_{\mathrm{lo}} \le r_{\mathrm{lo}}(3, 0.5) < -7.33$ on the whole domain D of Section 6.

The state v is not what actually ends the region from below. In every grid computed ($t \le 8$, $y \le 3$) and at the 48 points of Test A, that is the lowest state of the sector-0 block of charge -1 (with its mirror $+1$), a 2×2 block whose rows are in Appendix A. At the wider random fields of Test B it is so at 110 of 193 points (Section 8).

Proposition 5.4 (The sector-0 block of charge ± 1; proved for $H + GG^*$)**.** *Let $s = \sqrt{t}$, and let B be the block of charge -1 of $H + GG^*$ in the sector $j = 0$, on the states $(c_f, c_l) = (-1, 0), (0, -1)$. Let $P_{\mathrm{lo}}(x, y, s) = s^3 \det(B - \lambda_0 I)$. Then*

$$P_{\mathrm{lo}} = 2\big[(s^4 + 2s^2)x^3 + (-3s^3y^2 + 8s^3 + 10s)x^2 + (-4s^6 - s^4y^2 - 8s^4 - 2s^2y^2 + 4s^2 + 8)x + 4s^5y^2 + 3s^3y^4 - 8s^3y^2 - 14sy^2\big],$$

a cubic in x with positive leading coefficient, and the block of charge $+1$ has the same characteristic polynomial. If $x < r_1(y, t)$, the smallest real root of P_{lo}, then λ_0 is not the lowest eigenvalue of $H + GG^*$ in the sector 0. Hence the region of $H + GG^*$ lies in $x \ge r_1$.

Proof. The sector 0 of $H + GG^*$ is built as an exact 9×9 matrix from Q by a SymPy port of the general builder, with no closed-form rows. In the charge basis it is block diagonal: $q = \pm 2$ are 1×1 and equal λ_0, $q = \pm 1$ are 2×2, and $q = 0$ is 3×3. The determinant of the $q = -1$ block minus λ_0 gives P_{lo}, and the $q = +1$ block has the same characteristic polynomial (exact). A cubic with positive leading coefficient is negative below its smallest real root, so there the 2×2 matrix $B - \lambda_0 I$ has negative determinant, is indefinite, and B has an eigenvalue below λ_0 (`scripts/ricci_su2_lower_edge_closed_form.py`, receipt `research/edge-theorem-20261122-proofs/lower_edge_closed_form.json`). The closed-form rows at $j = 0$ equal this operator exactly. □

The proposition is stated for $H + GG^*$; the block is not shown to be gauge-orthogonal, and nothing here transfers to the gauge-orthogonal spectrum, for which r_{lo} is the proved bound. At each of the 48 points of Test A (computed): P_{lo} has three real roots; the trace of $B - \lambda_0 I$ at r_1 is at least 43.06, so r_1 is exactly the sector-0 edge there; the charge-0 block keeps a margin of at least 0.93 at r_1; and r_1 equals the measured lower end x_{lo} of the region in $j \le 12$ to 8.2×10^{-12}, about 1.61 or more above r_{lo}. At five sample points the smallest root is $r_1 = -4.134033$ at $(y, t) = (3, 3)$, -5.611733 at $(0.5, 3)$, -6.334165 at $(3, 10)$, -7.514047 at $(0.5, 10)$ and -5.759238 at $(1.5, 6)$; a scan of ϕ_A on $[-40, -1.5]$ turns non-negative at about these values. Every scan before the present work stopped at $x = -3$, which hid the lower end; the region had been read as a half-line.

Corollary 5.5 (The region is bounded)**.** *For each (t, y), every x at which the twist is the floor of every sector satisfies $r_{\mathrm{lo}}(t, y) \le x \le r_{\mathrm{hi}}(t, y)$, in both spectra. For $H + GG^*$ it also satisfies $\max(r_{\mathrm{lo}}, r_1) \le x \le \min(x_{12}^*, 0)$. Writing x_{lo} for the lower end of the region, $x_{\mathrm{lo}} \ge r_{\mathrm{lo}}$, and for $H + GG^*$, $x_{\mathrm{lo}} \ge r_1$.*

Proof. Propositions 5.3 and 5.4 and Corollary 5.2. □

This is the two-sided condition the title names. That the region is exactly one interval $[x_{\mathrm{lo}}, x^*]$, with no holes, is computed on grids and not proved. Figure 3 shows it at five stretches. Look at three things in it: the fill is one band at every height y; its left edge (solid) sits well to the right of the dashed proved bound r_{lo}; and its right edge changes colour with y, as the block that sets the upper edge changes from the near-top families at small y through $B_{3,1/2}$ to $B_{4,0}$ and, at large y and small t, back to a near-top family. What is proved about the band is narrower: Theorem 6.1 shows that the region contains $[-3, -1.5]$ for every $(t, y) \in [3, 10] \times [0.5, 3]$, and Theorem 5.6 gives, in the sectors $j \le 12$ on two slices, the exact upper end on $[-3, r_{\mathrm{next}})$.

5.3 The upper edge on two slices

Theorem 5.6 (The edge on two slices, sectors $j \le 12$; proved under (T))**.** *Let $t = 3$ and $y \in \{\sqrt{3}, 3/2\}$. Let x^* be the unique real root of $P_2(x, y, \sqrt{3})$ in $[-3, 1]$, and let r_{next} be the next real root above it of $\det(B_{4,0} - \lambda_4)$, a root of $P_1(x, y, \sqrt{3})$ (Proposition 4.1). Then:*

1. *$m(x) = \lambda_{\min}(B_{4,0}) - \lambda_4$ is positive on $[-3, x^*)$, zero at x^* and negative on (x^*, r_{next}), and x^* is a simple zero;*
2. *every charge block $B_{j,q}$ with $j \le 12$ other than $B_{4,0}$ and the two twist blocks has $\lambda_{\min}(B_{j,q}) > \lambda_j$ on $[-3, x^* + 0.02]$;*
3. *hence, for $x \in [-3, r_{\mathrm{next}})$, the twist is the lowest eigenvalue of $H + GG^*$ in every sector $j \le 12$ if and only if $x \le x^*$. It is the strict floor for $x < x^*$; at x^* the value λ_4 ties one eigenvalue of $B_{4,0}$.*

For $y = \sqrt{3}$, $x^* = -0.3821684822419167$ and $r_{\mathrm{next}} = -0.0650646510788456$; for $y = 3/2$, $x^* = -0.37158172515020627$ and $r_{\mathrm{next}} = -0.008268340671784679$.

Proof. Exact blocks, exact factorization on the slice, rational root isolation, interval Cholesky at $x = -3$ and on $[-3, x^* + 0.02]$, and Rellich's analytic branches; the five steps and Table 4 are in Appendix B.1. □

The theorem concerns $H + GG^*$ only. Its earlier form assumed that the closed-form blocks are the blocks of $H + GG^*$; that is now Lemma 2.3, and what remains is the transcription (T). The gauge-orthogonal edge on these slices is higher, at -0.3552 and -0.3516, and is not treated. The sectors $j > 12$ are open there; in $13 \le j \le 40$ every block keeps a gap of at least 5.50 (double precision).

5.4 Large sectors close to the edge

Theorem 5.7 (Large sectors on slabs; proved under (T))**.** *On each box of Table 5 (Appendix B.2), with the exact endpoints stated there, for every (x, y, t) in the box and every sector $j \ge 40$, every charge block of the sector other than the twist and its mirror has lowest eigenvalue greater than λ_j. On $[-3, -0.6] \times [0.5, 3] \times [3, 10]$ the same holds for every $j \ge 20$.*

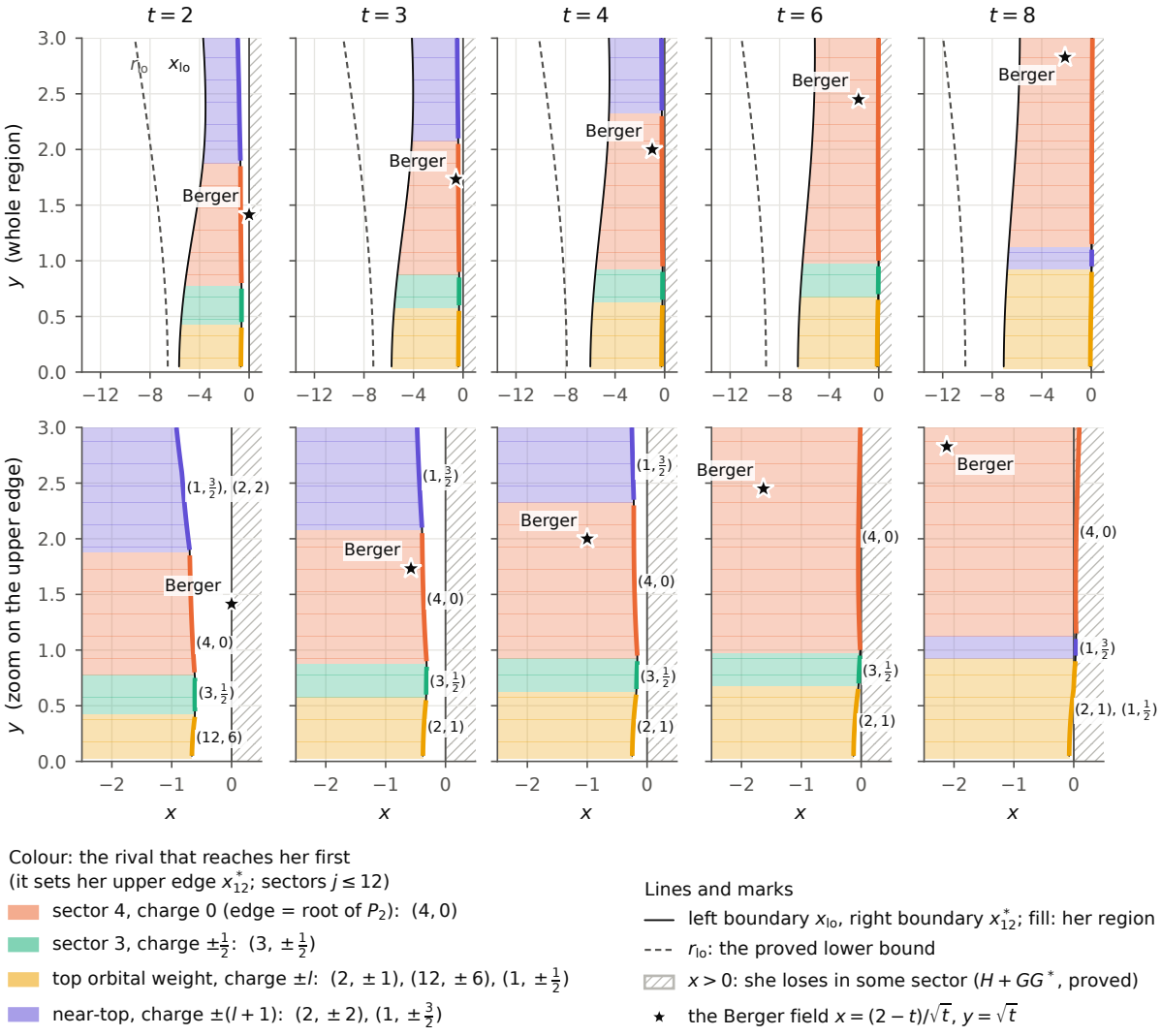

Figure 3. Her region in the sectors $j \le 12$ for $H + GG^*$ (computed, double precision). Panels: $t = 2, 3, 4, 6, 8$. Top row: the whole region. Bottom row: zoom on the upper edge. At each y (step 0.05 from 0.05 to 3), the fill runs from the lower edge x_{lo} to the upper edge x^*_{12}, the two sign changes of ϕ_A on a 0.05 grid over $x \in [-14, 1.5]$, refined by Brent's method to 10^{-12}. At all 300 pairs (t, y) there are exactly two sign changes, so in $j \le 12$ the region is one interval on this grid. The colour gives the block that sets x^*_{12}: $B_{4,0}$, $B_{3,1/2}$, or one of the two near-top families, $|q| = l + 1$ ($B_{1,3/2}$, $B_{2,2}$) and $|q| = l$ ($B_{2,1}$, $B_{1,1/2}$, $B_{12,6}$). The bottom row names each block. The lower edge is set at every pair by the sector-0 block of charge -1 (with its mirror; Proposition 5.4). The dashed curve is the proved bound r_{lo} of Proposition 5.3, from the state $\hat{\theta}^0 \otimes \tau_0$; it lies 0.91 or more below x_{lo}. Hatched: $x > 0$, where Theorem 5.1 proves for $H + GG^*$ that high sectors undercut her, so the all-sector region lies in $x \le \min(x^*_{12}, 0)$. The 47 positive x^*_{12} (all at $t = 8$, $y \ge 0.7$, at most +0.093) are cut-off artefacts. Star: the Berger field $x = (2 - t)/\sqrt{t}$, $y = \sqrt{t}$. At $t = 2$ the $j \le 12$ edge is not the all-sector edge at small y (Section 5.5). Upper edges agree with the competitor map `wp1_competitor_map.json` at its 60 shared grid points to 2.7×10^{-15}. Receipt `research/edge-paper-figures-20261122/region_j12.json`.

Proof. The blocks split into two kinds. *Near-end blocks* ($l-q \le N_1$ or $l+q \le N_1$, each with at most nine states) are scaled to $M = (B-\lambda_j)/l$, written in $U = 1/l$, and proved positive definite for all $U \in (0, 1/L_0]$ by interval $LDL^\top$ with bisection. *Bulk rows* use Gershgorin discs [26]: by Lemma 5.8 below, the interval-proved positivity of the quantity G on every row of a block gives $\lambda_{\min} > \lambda_j$ with no numerical step. The two blocks of charge $\pm(l+2)$ are 1×1 with entry exactly λ_j and are excluded. Details, parameters and run times are in Appendix B.2 (`scripts/edge_wp2_interval_proof.py`, receipts `research/edge-theorem-20261121/wp2_interval_proof_*.json`). □

Lemma 5.8 (Exact Gershgorin quantity; PROVED)**.** *For the closed-form rows as built by* `symbolic_rows` *(the rows of Lemma 2.3, under (T)), with x, y real, $t > 0$, and l, m symbolic: the blocks are real symmetric and conserve the charge; every off-diagonal entry of C has modulus $2|y||\sqrt{t}\,x - t - 2|/\sqrt{t}$, and every ladder entry has modulus $\sqrt{2}|y|$ or $\sqrt{2}\sqrt{t}$; the exact Gershgorin radius of the row (m, a) is $R_a + 2\sqrt{(l-m)(l+m+1)}\,P_a^- + 2\sqrt{(l+m)(l-m+1)}\,P_a^+$; and the quantity G evaluated by the interval proofs equals $D(m, a) - \lambda_{2l} - (\text{radius})$ exactly, for all nine types. The blocks of charge $\pm(l+2)$ are 1×1 with entry exactly λ_{2l} and radius 0, and every block with $|q| > l+2$ is empty. Hence, if $G > 0$ on every row of a block, its lowest eigenvalue exceeds λ_{2l}.*

Proof. Exact SymPy identities on the rows, including a check that the functions `FA` and `FB` of the proof code, run on symbolic arguments, return G (`scripts/ricci_su2_gershgorin_lemma_symbolic.py`, receipt `research/edge-theorem-20261122-proofs/gershgorin_lemma.json`, 34.9 s). As a cross-check (computed), G agrees with the Gershgorin quantities of the double-precision blocks on 23,031 rows to 1.0×10^{-12} relative. □

Four limits. The distances δ of Table 5 are measured from the worst grid point of each slab, so between grid points the distance to the edge is not proved. The sectors $j < 40$ on these boxes are not done, so the theorem does not by itself make the twist the floor there. The interval $x \in (-0.02, 0)$ is not covered. And the near-end matrices are tied to the rows only through (T): they agree with the blocks to 4.5×10^{-16} in double precision, not as a symbolic identity.

5.5 The all-sector edge

Conjecture 5.9. For $t \ge 3$ and $y > 0$, the all-sector edge of $H + GG^*$ equals $\min(x_{12}^*(t, y), 0)$.

The evidence for it lies in $3 \le t \le 12$, $0.25 \le y \le 3$: the competitor map, the tail checks above, and the near-top families below.

THE CONJECTURE FAILS AT AND NEAR $t = 2$ (DOUBLE PRECISION; TWO BUILDERS). The same statement on $2 \le t \le 12$ is false. At $t = 2$ exactly, the sector $j = 200$ undercuts the twist at the $j \le 12$ edge for $y = 0.25$ (margin -0.423) and for $y = 0.5$ (margin -0.0299), so the row $t = 2$, $y = 0.5$ of Table 1 is not the all-sector edge (`wp1_tail_check.json`). At $(t, y) = (2.01, 0.25)$, $x_{12}^* = -0.62410$. At $x = x_{12}^* - 5\times10^{-4} = -0.624598$, where ϕ_A over $j \le 12$ is still $+0.0052$, the block $q = 8$ of the sector $j = 16$ lies below λ_{16} by 0.00492, both from the blocks and from the general $H + GG^*$ builder (two eigenvalues below), and by 0.00353 in the gauge-orthogonal spectrum (two eigenvalues below; rechecked for this revision with the general builder). At $(2.001, 0.25)$, at $x = -0.64263$ and $x = -0.64513$, both below $x_{12}^* = -0.64213$, the sector $j = 58$ lies below by 0.2387 and 0.2109. A scan of $j \le 3000$ at $t = 2.001$, 2.01 and 2.03, $y = 0.25$ and 0.5, found an undercut only at $y = 0.25$ for $t = 2.001$ and 2.01 (`research/edge-theorem-20261121/workflow_reports.json`, the competitor-map rerun).

The mechanism: two near-top families. The blocks $q = l + 1$ (three states) and $q = l$ (six states) can be written with l symbolic. Their determinant numerators are $D_+(x, y, s, l)$, of degrees $(4, 4, 9, 3)$, and $D_0(x, y, s, l)$, of degrees $(8, 10, 19, 6)$, with $s = \sqrt{t}$ (checked numerically against the blocks to 6.8×10^{-13}). Their leading coefficients in l are

$$c_+ = -128\, s\, x\, (s-1)(s+1)(s^2-2),$$
$$c_0 = -65536\, s\, x\, (s-1)(s+1)(s^2-2)(3s^2-4)(sx-2s^2+2)(sx-s^2+2),$$

and both vanish identically at $s = \sqrt{2}$, that is at $t = 2$. Away from $t = 2$ the factor x pulls the family edges towards $x = 0$ as j grows. The factor $(sx - s^2 + 2)$ of c_0 vanishes at $x = (t-2)/\sqrt{t}$ (0.5774 at $t = 3$), so the statement that $x = 0$ is the only root of c_0 in the range of the edge holds only for $x \lesssim 0.5$. These polynomials and coefficients are exact algebra (`scripts/edge_wp1_block_polynomials.py`, receipts `wp1_top_family.txt`, `wp1_family_members.json`); the family edges are double precision. At $(t, y) = (12, 2)$ the edge of the family $q = l + 1$ falls roughly like $1/j$, from 0.2075 at $j = 12$ to 0.0028 at $j = 2000$ (Table 8, Appendix B.4). At $t = 2$ the family edges appear instead to converge to a negative limit: the family $q = l$ at $j = 2000$ gives -0.68467 for $y = 0.25$ and -0.61843 for $y = 0.5$.

Six of the eight competitors found in $j \le 12$ belong to these two families: D_+ at $l = \frac{1}{2}, 1, 6$ gives $(1, 3/2)$, $(2, 2)$ and $(12, 7)$; D_0 at $l = 1, 6$ gives $(2, 1)$ and $(12, 6)$; D_0 at $l = \frac{1}{2}$ gives $(1, 1/2)$ up to a spurious factor. Only $(4, 0)$ and $(3, 1/2)$ are sporadic. Because c_+ and c_0 vanish at $t = 2$, near $t = 2$ the families need not fall back to $x = 0$, and there they can take over from the $j \le 12$ competitors. That is what the failure shows, and it is why the conjecture is stated for $t \ge 3$ only.

6 The floor on a domain

Inside its region the twist can be proved to be the floor of every sector on a box of positive volume.

Theorem 6.1 (The floor on a domain; proved)**.** *On $D = \{x \in [-3, -1.5],\ y \in [0.5, 3],\ t \in [3, 10]\}$ the twist is the lowest eigenvalue of $H + GG^*$ in every sector, with multiplicity exactly two, and the lowest gauge-orthogonal eigenvalue there.*

It is also Theorem 7.3 of the version 3 draft of [6]; it is not in the published version 2.

Proof. (a) Reduction to charge blocks. By Lemma 2.3 each sector is the orthogonal sum of its charge blocks. The two twist blocks are 1×1 with entry λ_j (Proposition 3.2 and the antiunitary map). It suffices to show that every other block has lowest eigenvalue above λ_j on D. Then λ_j is the lowest eigenvalue of $H + GG^*$ with multiplicity exactly two, and since the twist is gauge-orthogonal and $H + GG^* = H$ on the slice, it is also the lowest gauge-orthogonal eigenvalue.

(b) Sectors $j \ge 80$. For the row $m = l - \xi$ of type a, $G = 4\xi(2l - \xi)(1 - 1/t) + lK_a + E_a -$ (ladder), built on (5). On D, $K_a > 0$ for every non-twist type. G is proved positive for all $l \ge 40$ on D by interval bisection, and by Lemma 5.8 this bounds every non-twist block above λ_j (`scripts/ricci_su2_family_large_j.py`, receipt `family_large_j.json`; details in Appendix B.3).

(c) Sectors $j < 80$. Every non-twist block is certified above λ_j on D by a mean-value interval certificate over 1,640,935 boxes, with no failure (`scripts/ricci_su2_family_block_cert.py`, receipt `family_block_cert_j80.json`, `all_certified` true). The final three scalar operations

of each box are done in round-to-nearest, and an a priori error bound shows that they cannot change any verdict (Appendix B.3). □

The certificate's per-box lower bounds are not spectral margins. The smallest, 1.22×10^{-6} in the sector $j = 1$, is the slack of the box on which the bisection stopped, so it reflects the stopping rule. The actual margin on D is about 2.35 or more (double precision; Remark 6.3).

Remark 6.2 (Why D stops at $x = -1.5$). Plain Gershgorin needs large l unless the domain stays away from the edge. At the near end of a sector ($\xi = 0$) the diagonal gap is lK_a, while the ladder coupling grows like $\sqrt{l}$, so plain Gershgorin needs l of order $1/K_a^2$, and K_a becomes small as $x \to 0$. Sampled cutoffs (double precision) are $l \approx 640$ for $x \in [-2, -0.5]$, $l \approx 160$ for $[-2, -1]$ and $l \approx 40$ for $[-3, -1.5]$. The near-end treatment of Theorem 5.7 is the route closer to the edge; it covers $j \geq 40$ up to about 0.02 below the grid edge, but the small sectors there remain to be certified (Appendix B.2).

Remark 6.3 (D lies inside the region). On D, $x \leq -1.5 < 0$, and $r_{\mathrm{lo}} < -7.33$ on all of D, so D sits well inside the bounds of Corollary 5.5. In double precision, $\min \phi_A$ at $x \in \{-3, -1.5\}$ over an 11×15 grid of D's (y, t) range is 2.35 ($j \leq 12$) and $\min \phi_S$ on a 3×3 grid is 2.69. These grid values are evidence only; the inclusion itself is settled by Theorem 6.1.

7 What decides the edge, and what does not

Three simpler readings of why the twist is the floor were tested (Tests 2, 4 and 5), each written down before its data, and each failed. A fourth test (Test 6), of a two-parameter model for the edge, failed in both of its pre-registered predictions.

Symmetry (Test 2; failed). The reading was that the rotation symmetry itself makes the maximal-charge state the floor. On the squashed meron, which has the same symmetry, the twist is an exact gauge-orthogonal eigenvector, yet it is the floor of no sector at any of the 2,600 pairs (t, j) checked (eigenvector residual at most 4.7×10^{-12}, $\|G^* b\| \leq 8.5 \times 10^{-15}$). The Berger field, run through the same code, became the floor of every sector $j \leq 12$ from $t = 2.70$. In two $SU(3)$ families with the Maurer–Cartan field $A = \frac{1}{2}\theta$, one stretching the $U(2)$ fibre and one the hypercharge circle, the extremal state is the floor of none of nine sectors at any of 200 grid points; one of the 1,800 point-sector pairs needed a fallback singular value routine. One difference, observed after the test and not pre-registered, is in the curvature term (Remark 3.6): on the twist's internal frame the field-strength share is $8 - 6t$ on the Berger field, but positive on the squashed meron. Tests 4 and 5 then showed that this term does not decide the floor (`scripts/ricci_su2_test2_family.py`, `scripts/ricci_su2_gyromagnetic_split.py`, receipts `test2_meron.json`, `su3_test2_family2a.json`, `su3_test2_family2b.json`, `gyromagnetic_split.txt`).

Alignment (Test 4; failed). The reading was that a field strength aligned with the twist's spin makes it the floor. For $A = s\theta$ on the round sphere, $s = 1.05, \ldots, 3.00$ (40 points), the field strength is aligned throughout (its field-strength share s_F on the twist's frame runs from -0.42 at $s = 1.05$ to -48 at $s = 3$). In $SU(2)$ the twist is the floor of $j = 0$ for $s \geq 1.5$ and of no sector $j \geq 1$ at any s; in the sector $j = 1$ the gap grows from 16.5 to 35.9. In $SU(3)$ it is the floor of the sector $(0, 0)$ for $s \geq 1.5$ and of no other (`scripts/ricci_alignment_test.py`, receipts `alignment_test_4a.json`, `alignment_test_4b.json`).

Alignment and the curvature term (Test 5; failed). The reading was that the twist is the floor when it alone spans the lowest eigenspace of R_0. On $A = s\theta$ over $(t, 1, 1)$, 72 points were classified from R_0 alone before any floor was computed: 35 singled out, 5 shared, 32 not lowest. The twist is the floor of every sector at none of them. At 34 of the 35 singled-out points it is the floor of $j = 0$ only; at $(s, t) = (1.25, 1.5)$ it is the floor of no sector. The gap grows with j (at $s = 1.5$, $t = 3$: 6.6, 12.6, 25.7, 41.1 for $j = 1, 2, 4, 8$) and shrinks with the stretch (at $j = 1$, $s = 1.5$: 13.8, 6.6, 2.1 at $t = 1.5, 3, 8$) (`scripts/ricci_stretch_test.py`, receipt `stretch_test.json`).

A model for the edge (Test 6; failed). The model $x^*(t) = c_1/t + c_2/t^2$ was fitted to the gauge-orthogonal edge of $j \le 12$ at $t = 2, 3, 4, 6$ and heights $y = 0.5$, 1.5, $\sqrt{t}$. Prediction E1 asked for agreement to 0.05 at held-out stretches. Interpolation held at 6 of 6 points ($t = 2.5$ and 5; errors -0.018, -0.038, -0.047, $+0.010$, $+0.024$, $+0.029$). Extrapolation to $t = 8$ held at $y = 0.5$ ($+0.033$) but failed at $y = 1.5$ (predicted -0.052, measured $+0.040$, error $+0.092$) and at $y = \sqrt{t}$ (predicted -0.041, measured $+0.138$, error $+0.179$). Prediction E2 failed: the model puts the Berger crossing at $t_c = 2.6315$, against $t^* \approx 2.6980$, a distance $0.067 > 0.05$ (`scripts/ricci_su2_edge_test.py`, receipts `edge_test_predictions.json`, `edge_test_results.json`). Two later findings bear on this test. The positive edges measured at $t = 8$ are artefacts of the cut-off $j \le 12$ (Section 5), and the region reported there as $[-3, x^*]$ is part of a region bounded below (Proposition 5.3).

Neutrality and blindness. A further reading is that the competitor is neutral, with total fibre charge zero, as the lowest state of $B_{4,0}$ is, and nearly blind to x. Data already in hand counted against neutrality before Test B: at $y = 0.5$ the competitors are blocks of non-zero charge (Section 4), and at 14 grid points with $y \ge 1.1$ and $x^*_{12} \le 0$ the competitor is $(1, \pm 3/2)$ or $(2, \pm 2)$ (`wp1_competitor_map.json`). Test B then counted against blindness: the competitor's slope ratio is at least 0.5 at 129 of 193 random fields (Section 8).

What does decide it. For $H + GG^*$, whether the twist is the floor of a sector is a comparison between λ_j and the lowest eigenvalues of the other charge blocks. For the gauge-orthogonal spectrum this comparison gives a sufficient condition, and the gauge-orthogonal edge lies slightly above (Test A: by 1.5×10^{-4} to 0.091). The structure of the comparison is exact. In every block, x enters the diagonal through $(w_a - 2m/\sqrt{t})^2$, with w_a affine in x; every entry of the remaining matrix C has degree at most one in x; and the ladder couplings do not involve x (Lemma 2.3). In the twist, x enters twice: by minimal coupling, through the fibre momentum κ, and by spin, through the field strength $B = y^2 - 2\sqrt{t}\,x$ along the fibre; the slope is $\partial_x \lambda = -2\kappa + 4\sqrt{t}$ (Section 3). The twist's slope near the edge is about 10. The competitor's depends on which block it is: $B_{4,0}$ is nearly flat at the three points of Section 4.2, but the charged competitors of Test B have slope ratios mostly above 0.5 (median 0.74, against 0.35 for the neutral ones; the neutral ones are below the threshold 0.5 in most sampled cases, but not all: 5 of 61 exceed it). So the edge is where the twist's value, bent by the field along her circle, meets whichever block reaches her first. An exploratory map, not pre-registered, agrees on the side: over $t = 1, 2, 3, 4, 6$, $x \in [-3, 3]$ (49 values), $y \in [0, 3]$ (37 values) and $j \le 8$, all 3,294 cells where the twist is the floor of all nine sectors have $x \le 0$, and 3,286 have $x < 0$ (`scripts/ricci_su2_twist_family_map.py`, receipt `twist_family_map.json`). This is consistent with Theorem 5.1.

The literature. The twist is a cousin of the unstable mode of a charged vector field in a homogeneous magnetic background [20], the classical face of the chromomagnetic instability

whose one-loop form appears in [22]; see also [25] for the standard usage. The flat-space mechanism is stated explicitly in [4] as a Landau-level energy plus a Zeeman term with gyromagnetic factor 2. The decomposition of λ in Section 3 has the same shape; I note the resemblance only, and no limit relating the two is proved. Instabilities of homogeneous backgrounds on the round S^3 are treated in [2, 12], and spectra on Berger spheres in [16, 10]. The closest is [2], on the negative modes of covariantly constant backgrounds, on the round sphere only. In the literature checked I found no edge of this kind and no Berger-sphere family of this kind; several classical full texts could not be read, so this is a statement about the search, not a priority claim.

8 Pre-registered tests A to F

Six further tests were written down, reviewed and fixed before any scored data were computed, as were Tests 2, 4, 5 and 6 of Section 7. Amendments fall into four kinds, each disclosed where it occurs. Most were made after a code gate fired (for Amendment C1, after a smoke test showed that a gate would fire) and before any scored quantity was computed. Test F's Amendment 1 (a peak test) was written after three of its 36 points had been printed, and is reported as not blind on those three. Test F's Amendment 2 (how to read the twist at a degenerate wall) was written after a gate stopped the run, before any further data. Its implementation correction was made after all 36 points and the scores had been seen; it is mechanical (it restores the registered rule), it recomputed nine wall points, and it changed no verdict. Both versions of those points are in the results note. This section gives each design in brief and its result. The full points, predictions, gates and amendments are in Appendix C. Every result here is computed.

Test A: the edge at held-out points of the family. 48 points (t, y) never computed before: 38 where P_2 was predicted to govern and 10 at small y. A1: the edge is the selected root of P_2, with competitor $B_{4,0}$, at the 38 points. A2: at small y the competitor is a block of the sector 2 or 3. A3: no sector $13 \le j \le 79$ undercuts the twist at three values of $x < 0$ in its region. A4: the region in $j \le 12$ is one interval on a 0.01 grid. Receipt `research/edge-theorem-20261121/wp4_heldout.json`. Every gate passed.

- *A1 failed at* 4 *of* 38 *points.* At the other 34 the competitor is $B_{4,0}$ and the measured edge equals the predicted root of P_2 to 1.35×10^{-12}. At three failures, at small stretch with a strong cross field, the block $(1, -\frac{3}{2})$ reaches the twist first; at the fourth, $(t, y) = (11, 1.2)$, the block $(12, -7)$ of the cut-off sector sets a positive edge in $j \le 12$ (Table 9, Appendix C). What holds is that P_2 governs where $B_{4,0}$ is the competitor.
- *A2 held* at all 10 small-y points: $(2, \pm 1)$ eight times and $(3, -\frac{1}{2})$ twice.
- *A3 held* at all 48 points, at the three tested values of $x < 0$; the smallest margin is +0.52.
- *A4 held* at all 48 points: the region in $j \le 12$ is a single interval on the 0.01 grid.

Descriptive: the lower end x_{lo} runs over $[-7.81, -3.64]$ and is set at every point by the sector-0 block of charge -1 (with its mirror); the gauge-orthogonal edge lies above the $H + GG^*$ edge at every point, by 1.5×10^{-4} to 0.091; the Test 6 model misses the measured edge by 0.076 on average and 0.20 at worst; and 20 of the 48 upper edges in $j \le 12$ are positive, the cut-off artefacts of Theorem 5.1.

Test B: general circle-symmetric fields. B-I, a code control, checks that 200 random members of the class of Proposition 2.1 ($k = \pm 1$, x, y and z free, $t \in [0.5, 15]$, a random constant gauge frame) behave as their reductions. B-II scans the reduced family over random (ρ, t), $\rho = \sqrt{y^2 + z^2}$, with the edge located on $x \in [-10, 10]$ in $j \leq 12$. Arms: B-half (exactly two sign changes of ϕ_A on a 0.01 grid), B-S (the competitor's slope ratio $\rho_s = |\partial_x \lambda_{\text{comp}}|/|\partial_x \lambda| < 0.5$ at every scored edge; the threshold was chosen after seeing three ratios, so a pass would have been weak evidence), and B-N (the competitor's charge, descriptive). Receipt `research/edge-theorem-20261121/wp4_general_fields.json`, final, under Amendment B1.

- *B-I passed* every gate at all 200 draws (B-sym 1.7×10^{-15}, B-exact 3.5×10^{-15}, B-red 2.2×10^{-14}, B-spec 3.9×10^{-15}, B-even 3.7×10^{-16}). As registered, this is a code control, not evidence. B-II-code passed under Amendment B1: in the final receipt the 27 known edges are reproduced to 2.4×10^{-13}, inside the gate's 10^{-9}.
- *B-count was met*: 193 of 200 points have an upper edge in $[-10, 10]$. The seven without one all have $t < 1$, squashed rather than stretched spheres.
- *B-half held* at all 193 points: the region in $j \leq 12$ is one interval on the 0.01 grid, over scored cross fields ρ from 0.33 to 8.27 and stretches from 1.0 to 15.0.
- *B-S failed* at 129 of 193 points, and at 70 of the 76 with $x_{12}^* \leq 0$. The quantiles of ρ_s (minimum, quartiles, maximum) are 0.002, 0.43, 0.67, 0.78, 0.88. Neutral competitors fail at 5 of 61 (median 0.35), charged ones at 124 of 132 (median 0.74).
- *B-N* (descriptive): 31.6% of the competitors are neutral. The most common is $(1, \pm\frac{3}{2})$, at 100 points, then $(4, 0)$ at 61.

Descriptive: x_{lo} runs from -8.89 to -2.92; it is set by the sector-0 block of charge -1 at 110 of 193 points, by $(1, \pm\frac{3}{2})$ at 54, by $(2, \pm 2)$ at 24, by $(3, \pm\frac{5}{2})$ at 4, and by the sector-0 block of charge 0 at one. 117 of the 193 upper edges in $j \leq 12$ are positive, cut-off artefacts for $H + GG^*$ by Theorem 5.1. The "nearly blind" reading of Section 4.2 therefore holds for $B_{4,0}$, not for the edge in general.

Figure 4 shows Tests A and B together. In panel (a), see the 34 points on the diagonal and the four diamonds below or beside it, where another block arrives first. In panel (b), see that every one of the 193 fields has a single bar, the interval, and that the open dots, the positive upper edges, are the large-stretch ones. In panel (c), see the neutral competitors mostly left of the threshold and the charged ones mostly right of it.

Test C: $SU(3)$ with a free fibre field. On $SU(3)$ with the metric that stretches the hypercharge circle (λ_8) by t, the left-invariant fields commuting with the joint frame-and-gauge action of $U(2)$ are, up to gauge, $M_a = uX_a$ $(a = 1, 2, 3)$, $M_8 = xX_8$, $M_a = yX_a$ $(a = 4, \ldots, 7)$, with x the field along the stretched fibre, now free. C-P1, existence: with x free, the region where the twist is the floor of all nine listed sectors (gauge-orthogonal spectrum) is non-empty, strictly at every grid point with $t \geq 3$, weakly at one point at least. C-P2 to C-P5 ask about the side, the interval, the slope and the edge against t. The grid is $t \in \{2, 3, 4, 6, 8\}$ by $(u, y) \in \{(\frac{1}{2}, \frac{1}{2}), (\frac{1}{2}, 1), (1, 1), (1, 2)\}$, 20 shapes, the nine sectors of Test 2, and x in steps of 0.25 on $[r_{\text{lo}} - 0.5,\ r_{\text{hi}} + 0.5]$. Every claim of Test C is about the nine listed sectors on that grid. Receipt `research/edge-theorem-20261121/wp4_su3_free_fibre.json`. Every gate passed, among them C-K4 (the $SU(2)$ analogue: coefficient of x^2 equal to 1 to 3×10^{-14}, three known edges to

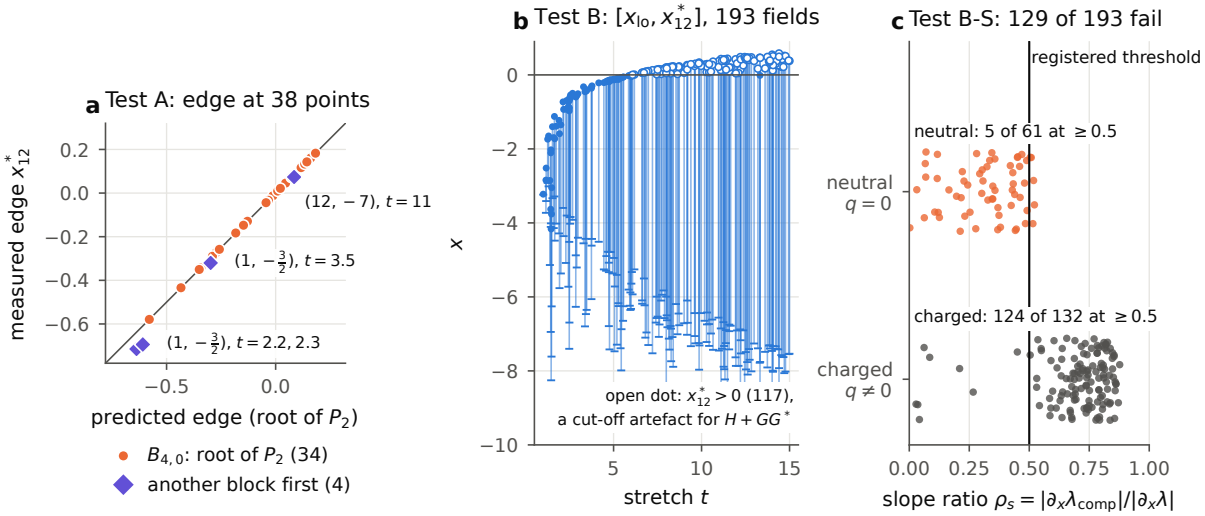

FIGURE 4. Pre-registered Tests A and B (computed). (a) Test A at the 38 points outside the small-y class: predicted edge (the root of P_2 selected under Amendment 1) against the measured edge in $j \leq 12$. At 34 points the competitor is $B_{4,0}$ and the two agree to 1.35×10^{-12}. At 4 points (diamonds) another block reaches her first: $(1, -3/2)$ at $t = 2.2$, 2.295 and 3.5, and $(12, -7)$ at $t = 11$, where the measured edge is positive. Both blocks belong to the near-top family $|q| = l + 1$. (b) Test B: her interval $[x_{lo}, x^*_{12}]$ in $j \leq 12$ at the 193 scored general circle-symmetric fields, against the stretch t. Bar: the interval. Dot: x^*_{12}. Tick: x_{lo}. Open dots: the 117 fields with $x^*_{12} > 0$, which for $H + GG^*$ are cut-off artefacts by Theorem 5.1. The lower edge is set by the sector-0 block of charge -1 at 110 of the 193. (c) Test B-S: the competitor's slope ratio ρ_s at each scored edge, for neutral ($q = 0$, all $B_{4,0}$) and charged competitors, with the registered threshold 0.5. B-S fails: 129 of 193 have $\rho_s \geq 0.5$ (5 of 61 neutral, 124 of 132 charged; 70 of the 76 with $x^*_{12} \leq 0$). The "nearly blind" reading holds for $B_{4,0}$, not in general. Receipts `wp4_heldout.json` and `wp4_general_fields.json`.

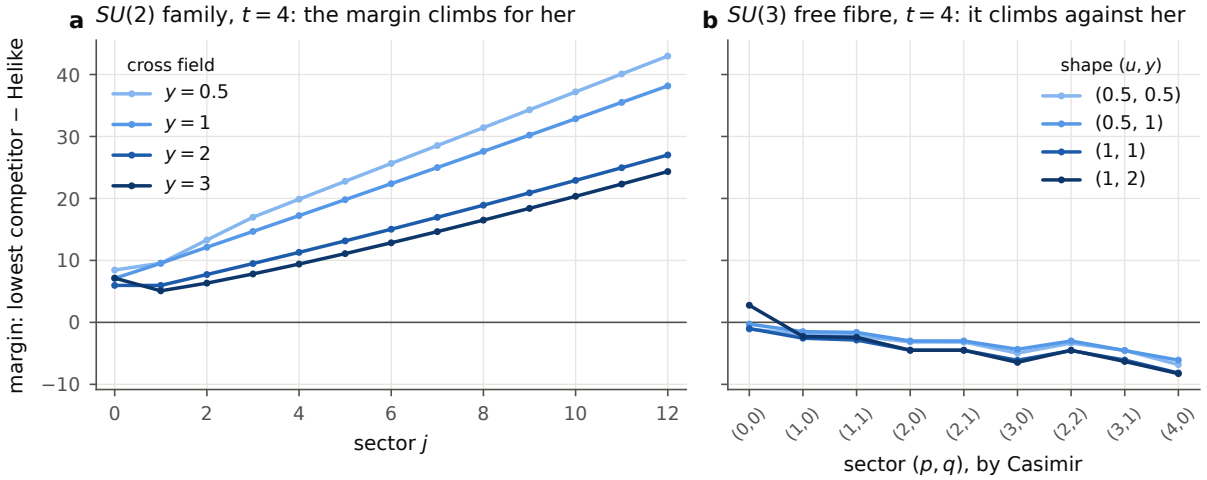

Figure 5. The lift climbs for her in $SU(2)$ and against her in $SU(3)$ (computed, double precision, gauge-orthogonal spectrum, $t = 4$, shared vertical scale). (a) The $SU(2)$ family at $y = 0.5, 1, 2, 3$: in each sector $j \le 12$, the lowest gauge-orthogonal eigenvalue other than her two copies, minus λ_j. Each curve is taken at the x that maximises the worst sector ($x = -3.02, -2.96, -2.52, -3.06$). Every margin is positive, the smallest being 8.45, 7.10, 5.97, 5.09, and from $j = 2$ on they grow with j. (b) The post-hoc diagnostic of Test C, the $SU(3)$ family with a free fibre field, at the four shapes (u, y). The same margin in the nine sectors, ordered by Casimir, at the best x of a 0.25 grid. It is negative in every sector at three shapes and in every sector except $(0, 0)$ (+2.76) at $(u, y) = (1, 2)$. It falls with the sector to about -6 to -8.3 in $(4, 0)$. Panel (b) is post-hoc and not part of the registered protocol. Receipts `research/edge-paper-figures-20261122/su2_margins_t4.json` and `wp4_su3_diagnostic_posthoc.json`.

3×10^{-9}), C-quad (the twist's coefficient of x^2 is $q_8^2 = 3/4$ in all nine sectors at all 20 shapes) and C-lin (the bounding state is affine in x, exactly).

- *C-P1 failed, weakly and strictly.* At none of the 20 shapes is the twist the floor of all nine listed sectors at any x of the 0.25 scan, for either spectrum (outside the scan the affine bounding state excludes it). By the rule fixed in advance this counts against the reading of Section 9 beyond $SU(2)$, in this family.
- C-P2 is not informative, and C-P3, C-P4 and C-P5 are vacuous, because there is no region.

A diagnostic run after the verdict, and not part of the protocol (`wp4_su3_diagnostic_posthoc.json`), shows how far the twist is from the floor. At $t = 4$, at the x that maximises its worst margin over the sectors, the margin is negative in every sector at three of the four shapes, and in every sector other than $(0, 0)$ at $(u, y) = (1, 2)$. It grows more negative with the sector, from -1.5 to -2.6 in $(1, 0)$ to -6.1 to -8.3 in $(4, 0)$, and $(4, 0)$ is the blocking sector at 121 of the 123 values of x scanned (the other two: $(3, 1)$). Figure 5 sets this beside $SU(2)$ on the same scale: in panel (a), see the $SU(2)$ margins stay positive and climb with the sector; in panel (b), see the $SU(3)$ margins fall below zero and keep falling. In $SU(2)$ the field along the circle gives the twist a discount on the lift to higher sectors (Corollary 3.3). In this $SU(3)$ family the higher sectors cost it more at every x scanned. What carries over is structural: the coefficient of x^2 is the squared charge, and the bounding state is affine.

Test D: $SU(3)$ stretched along the twist's own charge circle. Test C stretched the hypercharge circle. Its write-up named the obvious next test, and Test D is it: stretch $SU(3)$ along the circle of the twist's own charge, $H = -i\,\mathrm{diag}(1, 0, -1)$. It was chosen after Test C failed; it is a new hypothesis and does not rescue Test C. The metric is t on $e_H = \frac{1}{2}X_3 + \frac{\sqrt{3}}{2}X_8$ and 1 on the other seven directions. The registered sub-family has five parameters, $M_{e_H} = x\,e_H$, $M_{e_K} = w\,e_K$ and the root planes $(1,2)$, $(2,3)$, $(1,3)$ at strengths y_{12}, y_{23}, y_{13}, with x the field along her own circle; it is not the whole symmetric class. The grid is $t \in \{2, 3, 4, 6, 8\}$ by four shapes $(w, y_{12} = y_{23}, y_{13})$, the nine sectors of Test 2, and x on a 0.25 grid with a golden-section search wherever the grid finds no region. The predictions are D-P1 (existence, weak and strict), D-P2 (her floor set lies on the side $x \le 0$, scored only where neither the bound nor a truncation artefact forces it), D-P3 (one interval), D-P4 (the competitor's slope ratio, post hoc) and D-P5 (descriptive). A pass of D-P1 is reported as truncation-sensitive unless two further sectors confirm it. The design was revised after an adversarial review, before any floor, edge or competitor of the family was computed (`research/edge-theorem-20261122-d/wp5_prereg_D_su3_own_circle.md`; details in Appendix C).

Results (computed; receipt `research/edge-theorem-20261122-d/wp5_su3_own_circle.json`). Every gate passed: the Test C controls, the rotated-basis and wrong-axis controls (7.7×10^{-15} and 3.0×10^{-14}), D-quad (5.3×10^{-15}), D-kappa, D-sym ($\|[Q, H]\|$ to 6.4×10^{-15}), D-lin, D-mult and D-bound. Along her own charge circle the twist is the floor of all nine listed sectors at 19 of the 20 shapes, and at all 16 with $t \ge 3$: D-P1 held, weakly and strictly. The pass survives the two additional sectors tested, $(5, 0)$ and $(6, 0)$, which does not rule out an obstruction from a still higher sector. At one shape with $t = 2$ the sectors $(5, 0)$ and $(6, 0)$ remove every grid point of her region, and at every other non-empty shape between 2 and 8 grid points survive them. D-P2 held at all 15 scorable shapes (her region lies at $x < 0$ at all 19). D-P3 held: one interval at every non-empty shape. D-P4 failed: the competitor at the upper edge is the neutral block $(3, 0)$, with slope ratio 0.15 to 0.19, or the charged block $(4, 0)$, with charge -7 and slope ratio 0.61 to 0.76; the charged one takes over as t grows. Hypercharge (Test C) and her own charge circle (Test D) differ only in the stretched circle, and the twist is the floor nowhere along the first and almost everywhere along the second. Every clause of the reading except the blind competitor carries over to this $SU(3)$ slice along her own circle: exactness, minimal coupling with charge 1, the lift slope $(p + q)/\sqrt{t}$, the bounded region in one interval, and the side. In $SU(3)$ her charge circle is at once the principal circle, the coroot of her highest root and a regular circle; which of these she needs is the question of Test F.

Test E: for $x > 0$, who holds the floor. Theorem 5.1 shows that for $x > 0$ the twist is not the floor of every sector, and names a state that undercuts her: e_-, of weight $m = l$ and type $(1, -1)$ in the block $B_{2l,l}$, whose internal turning is opposite to the field along the circle relative to its own orbital turning ($c_l\, m\, x < 0$). Test E asked whether that state, and not some other, actually holds the floor. At 60 scored points ($y > 0$, $t \ge 3$, sectors $j \le 400$), the floor eigenspace is at least half across-reaching from some $j_0 \le 272$ on, and from $j = 1$ at most points (E1, held at 60 of 60). Its admixture of other types matches the first-order mixing predicted from the rows of its own block: the ratio of measured to predicted lies in $[0.86, 1.00]$ (E3, held at 60 of 60). The registered onset-scaling arm could not be scored (four eligible pairs; descriptively their ratios are 4.41 to 4.61, against a predicted 4). At $t = 2$ a different across-reaching block, $\pm(l - 2)$, holds the floor at 15 of 20 points.

So the statement "a state that turns against the field holds the floor" survives at $t = 2$, but the identification with e_- does not. The code gates (block against full builder, her block against λ_j, the exact state at $y = 0$, the mirror blocks) pass at 6×10^{-15} or better. Script `edge_wp6_two_hands.py`, receipt `research/edge-theorem-20261122-e/wp6_two_hands.json`.

Test F: which circle. Test F sweeps the stretched circle across the Weyl chamber of $Sp(2)$ and a line through the chamber of $SU(4)$, at six angles from the coroot $\theta^\vee$ of her highest root (0°, a wall) through the principal circle $\rho^\vee$ (18.43°) to the far wall (45°), at $t = 3$ and three shapes. Her cell *lives* if her floor region is non-empty and survives the extra sectors at two or more shapes. Its known-answer gates reproduce Tests D and C to 3.3×10^{-15} and 2.1×10^{-14}. She lives at 0° and 9.22° in both groups (H_θ supported). At $\rho^\vee$ she is marginal in $Sp(2)$ (1 of 3) and absent in $SU(4)$; she is absent at 27.65° and 36.87° in both. So the principal-circle hypothesis H_P and the regular-circle hypothesis $\mathrm{H}_{\mathrm{reg}}$ are refuted. A peak test added by amendment (her best margin largest at $\rho^\vee$) is refuted too: her margin peaks at 9.22° in $Sp(2)$ and at 0° in $SU(4)$, at all three shapes. Her region lies on the side against her charge at all 13 scorable cells. She also lives at the far wall of $Sp(2)$, which is the coroot of the short highest root; this was not predicted. There her state is not purely a twist: in the trivial sector 32 to 46% of it is the short root's twist and the rest mixes the two long top roots (a post-hoc diagnostic), and the field y_θ sat on the short root's plane by the code's tie-break. Two amendments (a peak test, and the reading of her state at a wall where the top charge is degenerate) and a disclosed correction of the second one's implementation are recorded with what had been seen; the correction changed no verdict. Reading: what carries the edge law between groups is the circle of her own $SU(2)$.

9 Scope and open problems

Scope. The results concern the classical linearised operator. Both the L^2 (Coulomb) slice and $H + GG^*$ are given, and where only one is proved the text says which. Nothing here is a statement about the quantum theory or a mass gap. Most members of the family are not Yang–Mills critical points, so the edge describes the landscape at a field, not a dynamical transition; at the Berger field the Yang–Mills flow moves away faster than any twist grows ([6], "Further observations"). The stability theorems for Yang–Mills fields [5, 21, 14, 23] and the recent floor-type estimate for abelian Yang–Mills–Higgs fields on the round sphere [11] concern critical points. The class of fields is the one of Proposition 2.1: left-invariant, symmetric under the right circle about the long axis lifted by a constant gauge circle. Outside D and the two slices of Theorem 5.6, every statement about the region is computed in $j \le 12$ or bounded by Theorems 5.1 and 5.7 and Propositions 5.3 and 5.4.

Open problems.

1. *The all-sector edge as a theorem.* Conjecture 5.9 for $t \ge 3$. The "if and only if" on $(-1.5, x^*]$ in every sector: $j > 12$ is open on the slices of Theorem 5.6, $x \in (-0.02, 0)$ is not covered by Theorem 5.7, and the small sectors $j < 40$ on its boxes are not certified. The gauge-orthogonal edge in exact form, and a gauge-orthogonal version of Theorem 5.1.
2. *The transcription (T).* A symbolic check of the near-end matrices of the slab proof and of the slice construction would turn the two remaining proved under (T) results (Theorems 5.7 and 5.6) into proved.

3. *Near $t = 2$.* The near-top families take over there (c_+ and c_0 vanish at $s = \sqrt{2}$). The all-sector edge near $t = 2$ is unknown.
4. *The lower edge.* The sector-0 edge is the smallest root r_1 of the cubic P_{lo} wherever the trace of $B - \lambda_0 I$ is positive there; that is checked at 48 points, not proved over a domain. That no sector $j \geq 1$ cuts in earlier is computed at those points and false at some Test B fields, where blocks of the sectors 1 to 3 set the lower end. The one-interval structure is computed on grids but not proved.
5. *Fields that mix sectors.* Circle-invariant fields that are not left-invariant, lifts by non-constant gauge transformations, other circles. There the twist is no longer alone in its charge block, so its exactness is itself open.
6. *Other groups.* In the $SU(3)$ family of Test C, stretched along the hypercharge circle, the twist is the floor of all nine listed sectors at none of the 20 shapes on the scan (step 0.25, double precision); at $t = 4$ the post-hoc margins in $(4, 0)$ are about -6 or lower. Whether a family stretched along the circle of the twist's own charge behaves like $SU(2)$ was the question of Test D: it does, at 19 of 20 shapes in that slice (Section 8). Which circle is needed in general (the principal circle, the coroot of her highest root, or any regular circle) was the question of Test F: in $SU(4)$ and $Sp(2)$ it is the coroot of her highest root, and not the principal circle. Why she returns at the far wall of $Sp(2)$ is open. Three readings (the short highest root's own circle, a corner ray of the chamber, or the short root tied at the top) predict different outcomes on three circles of $Sp(3)$; a further pre-registered test (Test G) separates them and replicates Test F in G_2 and $Sp(3)$. It is running.
7. *Competitors in closed form.* The block $(3, 1/2)$ has one edge factor of degrees $(11, 14, 26)$, irreducible over $\mathbb{Q}$. The polynomials of the small-y blocks are known, but no two-dimensional region theorem at small y is.
8. *A reading.* The decomposition of λ invites reading the edge as the point where the field along the long circle turns against the twist's charge by enough, but not too much, as the shape of space sets. That is a hypothesis, not a result, and Test C shows that it does not hold in every family I have tested.

10 Data, receipts and reproducibility

Every claim of this paper has a script that produces it and a receipt that records its output. Scripts are in `scripts/`. Receipt directories are abbreviated: `F` is `research/su2-floor-family-20261119/`, `E` is `research/edge-theorem-20261121/`, `P` is `research/edge-theorem-20261122-proofs/`, `G` is `research/edge-paper-figures-20261122/` `D` is `research/edge-theorem-20261122-d/`, `H` is `research/edge-theorem-20261122-e/` and `W` is `research/edge-theorem-20261122-f/`. The status column uses the labels of Section 1: proved, computed, proved under (T). The scripts run with Python, NumPy, SymPy [24] and mpmath [19], one thread (`OMP_NUM_THREADS=1`).

claim	script	receipt	status
Prop. 2.1 (class reduces to the family)	`edge_wp4_design_checks.py`	`E/wp4_design_checks.json`	PROVED (algebra); maps COMPUTED
Lemma 2.2 (Weitzenböck identity, Ricci, F)	`ricci_su2_weitzenbock_family_symbolic.py`	`P/weitzenbock_family.json`	PROVED
Lemma 2.3 (charge blocks, rows)	`ricci_su2_weitzenbock_family_symbolic.py`, `ricci_su2_exact_edge.py`	`P/weitzenbock_family.json`, `F/charge_selection_symbolic.txt`	PROVED
Code rows = proved rows (exact)	`ricci_su2_rows_transcription_check.py`	`P/rows_transcription.json`	PROVED
Condition (T) (near-end and slice objects)	`ricci_su2_weitzenbock_family_symbolic.py`, `ricci_su2_exact_edge.py`	`P/weitzenbock_family.json` (part 3), `F/exact_edge.json`	COMPUTED
Prop. 3.1 (twist exact)	— (counting)	—	PROVED
Prop. 3.2 (closed form)	`ricci_su2_twist_family_closed_form.py`, `ricci_su2_direct_rayleigh.py`	`F/twist_family_closed_form.txt`, `P/direct_rayleigh.json`	PROVED
Prop. 3.4 (anatomy)	`ricci_su2_twist_anatomy.py`; Lean `Price.lean`	`F/twist_anatomy.json`	PROVED
Rem. 3.6 (shares on the meron)	`ricci_su2_gyromagnetic_split.py`	`F/gyromagnetic_split.txt`	COMPUTED
Edge table, Berger crossings	`ricci_su2_exact_edge.py`	`F/exact_edge.json`	COMPUTED
Competitor slopes, monotone grid	`ricci_su2_twist_anatomy.py`	`F/twist_anatomy.json`	COMPUTED
Prop. 4.1 (edge polynomial)	`ricci_su2_edge_polynomial.py`, `edge_wp1_block_polynomials.py`; Lean `Edge.lean`	`F/edge_polynomial.txt`, `.srepr`; `E/wp1_block_polynomials.json`	PROVED
Prop. 4.2 (Berger restriction)	Lean `Edge.lean` (`edgeFactor_berger`)	Lean build	PROVED
P_1, P_2 on the grid edges	`edge_wp1_block_polynomials.py`	`E/wp1_poly_check_final.json`	COMPUTED
Competitor map, Table 3	`edge_wp1_competitor_map.py`, `edge_wp1_block_polynomials.py`	`E/wp1_competitor_map.json`, `.md`, `wp1_block_polynomials.txt`	map COMPUTED; polynomials PROVED
Thm. 5.1 ($x > 0$ loses, $H + GG^*$)	`ricci_su2_direct_rayleigh.py`, `edge_wp2_symbolic.py`	`P/direct_rayleigh.json`, `E/wp2_symbolic.txt`	PROVED

claim	script	receipt	status
Positive edges are artefacts	`edge_wp1_competitor_map.py`	`E/wp1_tail_check.json`, `wp1_tail_negx.json`, `wp1_fullsector_check.json`, `workflow_reports.json`	COMPUTED
Prop. 5.3 (r_{lo}, r_{hi})	`ricci_su2_direct_rayleigh.py`, `edge_wp4_design_checks.py`	`P/direct_rayleigh.json`, `E/wp4_design_checks.json`	PROVED
Prop. 5.4 (cubic P_{lo}, bound r_1)	`ricci_su2_lower_edge_closed_form.py`	`P/lower_edge_closed_form.json`	PROVED ($H + GG^*$)
$r_1 = x_{\mathrm{lo}}$ at the Test A points	`ricci_su2_lower_edge_closed_form.py`	`P/lower_edge_closed_form.json`	COMPUTED
One interval (Fig. 3)	`edge_paper_figures.py`	`G/region_j12.json`	COMPUTED
Thm. 5.6 (two slices)	`edge_wp3_slice_iff.py`	`E/wp3_slice_iff.json`, `.md`, `_log.txt`	PROVED under (T)
Lemma 5.8 (exact Gershgorin G)	`ricci_su2_gershgorin_lemma_symbolic.py`	`P/gershgorin_lemma.json`	PROVED
Thm. 5.7 (slabs, $j \geq 40$)	`edge_wp2_interval_proof.py`	`E/wp2_interval_proof_*.json`, `wp2_verify_rerun_x-0.6_L20.json`	PROVED under (T)
Conj. 5.9 fails near $t = 2$	`edge_wp1_competitor_map.py`	`E/wp1_tail_check.json`, `workflow_reports.json`	COMPUTED
Near-top families D_+, D_0	`edge_wp1_block_polynomials.py`	`E/wp1_top_family.txt`, `wp1_family_members.json`	algebra PROVED; edges COMPUTED
Thm. 6.1 (floor on D), $j \geq 80$	`ricci_su2_family_large_j.py`	`F/family_large_j.json`	PROVED
Thm. 6.1, $j < 80$	`ricci_su2_family_block_cert.py`, `ricci_su2_outward.py`	`F/family_block_cert_j80.json`	PROVED
Rounding bound for the $j < 80$ certificate	`ricci_su2_family_cert_rounding_bound.py`	`P/rounding_bound.json`, `rounding_bound.md`	PROVED
Rem. 6.3 (margins on D)	`ricci_su2_family_large_j.py`, `ricci_su2_exact_edge.py`	`F/family_large_j.json`	COMPUTED
Tests 2, 4, 5, 6	`ricci_su2_test2_family.py`, `ricci_su3_test2_family.py`, `ricci_alignment_test.py`, `ricci_stretch_test.py`, `ricci_su2_edge_test.py`	`F/test2_*.json`, `su3_test2_*.json`, `alignment_test_*.json`, `stretch_test.json`, `edge_test_*.json`	COMPUTED
Exploratory map	`ricci_su2_twist_family_map.py`	`F/twist_family_map.json`	COMPUTED

claim	script	receipt	status
Test A	`edge_wp4_points.py`, `edge_wp4_heldout.py`	`E/wp4_heldout.json`, `wp4_heldout_log.txt`; prereg `wp4_prereg_A_heldout.md`, `wp4_prereg_A_points.json`	COMPUTED
Test B	`edge_wp4_general_fields.py`	`E/wp4_general_fields.json`, `wp4_general_fields_log.txt`; prereg `wp4_prereg_B_general_fields.md`	COMPUTED
Test C	`edge_wp4_su3_free_fibre.py`	`E/wp4_su3_free_fibre.json`, `wp4_su3_free_fibre_log.txt`; prereg `wp4_prereg_C_su3.md`	COMPUTED
Test C diagnostic (post hoc)	`edge_wp4_su3_diagnostic.py`	`E/wp4_su3_diagnostic_posthoc.json`, `wp4_su3_diagnostic_posthoc_log.txt`	COMPUTED
Test D	`edge_wp5_design_checks.py`, `edge_wp5_su3_own_circle.py`	`D/wp5_prereg_D_su3_own_circle.md`, `wp5_design_checks.json`, `wp5_su3_own_circle.json`	COMPUTED
Test E	`edge_wp6_two_hands.py`	`H/wp6_prereg_E_two_hands.md`, `wp6_two_hands.json`	COMPUTED
Test F	`edge_wp7_principal_circle.py`, `edge_wp7_groups.py`	`W/wp7_prereg_F_principal_circle.md` and its two amendments, `wp7_principal_circle.json`	COMPUTED
Figures 1–5	`edge_paper_figures.py`	`G/region_j12.json`, `berger_path.json`, `su2_margins_t4.json`	COMPUTED (Fig. 1: closed forms)
Lean theorems (16)	`docs/papers/berger-spectrum/lean/Helike/`	`README.md`, `RESULTS.md`, `Axioms.lean`	PROVED (polynomial identities)

Reproducing. Each script writes its receipt to the path above, given as its argument (two have it as a default). The symbolic proofs run in under a minute each (21.7 s for Lemma 2.2, 34.9 s for Lemma 5.8). The domain certificate for $j < 80$ takes about 63.6 CPU-hours; the slab proofs take from 19 s to about 4,446 s per box. The results notes of the pre-registered tests are `docs/research/edge-prereg-A-results-2026-11-22.md` and its siblings for B, C, D, E and F; the notes of the earlier tests are in `docs/research/`.

Funding and competing interests

This work received no funding. The author declares no competing interests.

Code and data availability

All programs, certificates and receipts are in the GIGI repository, `https://github.com/nurdymuny/gigi` (tag `edge-paper-v1.1`); Section 10 lists them claim by claim. The sixteen Lean theorems are in `docs/papers/berger-spectrum/lean/Helike/Price.lean` and `Edge.lean`, with `README.md` and `RESULTS.md`. They depend only on the axioms `propext`, `Classical.choice` and `Quot.sound`, build with `lake exe cache get` and `lake build`, and `lake env lean Axioms.lean` lists the axioms. They are on the branch `feat/helike-lean`, tagged `edge-paper-v1-lean`. This paper, its source, and the code and data above are archived on Zenodo.

A Charge-block rows and competitor polynomials

Fibre rotations. The values $w_a = c_f(t-2)/\sqrt{t} - c_l\,x$ of (3) are:

(c_f, c_l)	w_a	(c_f, c_l)	w_a
$(1,1)$	$\sqrt{t} - x - 2/\sqrt{t}$	$(0,0)$	0
$(1,0)$	$(t-2)/\sqrt{t}$	$(0,-1)$	x
$(1,-1)$	$\sqrt{t} + x - 2/\sqrt{t}$	$(-1,1)$	$-\sqrt{t} - x + 2/\sqrt{t}$
$(0,1)$	$-x$	$(-1,0)$	$(2-t)/\sqrt{t}$
		$(-1,-1)$	$-\sqrt{t} + x + 2/\sqrt{t}$

Every entry of C has degree at most one in x, and the ladder couplings $\Omega_\pm$ do not involve x (exact; receipt `wp4_design_checks.json`). On the Berger path $w_a = c\,(t-2)/\sqrt{t}$ and every nonzero entry of $\Omega_\pm$ has modulus $\sqrt{2t}$ (`charge_selection_symbolic.txt`). The exact w, C and $\Omega_\pm$ are stored in `weitzenbock_family.json`.

Moduli (Lemma 5.8). Every off-diagonal entry of C has modulus $2|y|\,|\sqrt{t}\,x - t - 2|/\sqrt{t}$. The number of same-charge partners of a row is 0 for the types $(\pm1,\pm1)$, 2 for $(0,0)$ and 1 for every other type. Every ladder entry has modulus $\sqrt{2}|y|$ or $\sqrt{2}\sqrt{t}$. The column sums R_a, P_a^-, P_a^+ match the ingredients of `ricci_su2_family_large_j.py` for all nine types (`gershgorin_lemma.json`).

The sector-0 block of charge -1. On the states $(c_f, c_l) = (-1,0), (0,-1)$, with $s = \sqrt{t}$, the block of $H + GG^*$ in the sector 0 is

$$B = \begin{pmatrix} 2(s^2y^2+2)/s^2 & -2y(sx - s^2 - 2)/s \\ -2y(sx - s^2 - 2)/s & 4s^2 + x^2 + y^2 \end{pmatrix},$$

and $\operatorname{tr}(B - \lambda_0 I) = 4s^2 - x^2 - x(4s + 8/s) + 5y^2 - 4/s^2$ (`lower_edge_closed_form.json`). Its upper-left entry does not depend on x, while λ_0 grows like x^2; that is the mechanism of the lower edge.

Table 3. Blocks that set the edge in the sectors $j \le 12$ (map computed; polynomials exact). Degrees are in (x, y, s); "$s\cdot$" marks a factor s split off. †: block of the top sector allowed, a cut-off artefact. Receipts `research/edge-theorem-20261121/wp1_competitor_map.md` and `wp1_block_polynomials.txt`.

block	size	entries in	edge factor	terms	grid edges	max |root − edge|
$(4, 0)$	9	$\mathbb{Q}(\sqrt{2}, \sqrt{3})$	P_2, $(7, 8, 16)$	113	77	2.4×10^{-13}
$(3, \frac{1}{2})$	8	$\mathbb{Q}(\sqrt{2}, \sqrt{6})$	$(11, 14, 26)$	400	6	1.4×10^{-14}
$(2, 1)$	6	$\mathbb{Q}$	$s \cdot (8, 10, 18)$	169	20	2.3×10^{-13}
$(1, \frac{1}{2})$	5	$\mathbb{Q}(\sqrt{2})$	$s \cdot (7, 10, 16)$	133	4	1.5×10^{-16}
$(1, \frac{3}{2})$	3	$\mathbb{Q}(\sqrt{2})$	$s \cdot (4, 4, 8)$	26	15	8.5×10^{-14}
$(2, 2)$	3	$\mathbb{Q}$	$s \cdot (4, 4, 8)$	27	2	1.7×10^{-14}
$(12, 6)^{\dagger}$	6	$\mathbb{Q}(\sqrt{6}, \sqrt{11})$	$s \cdot (8, 10, 18)$	172	1	1.7×10^{-15}
$(12, 7)^{\dagger}$	3	$\mathbb{Q}(\sqrt{6})$	$s \cdot (4, 4, 8)$	27	7	1.1×10^{-13}

Competitors. Table 3 lists the eight blocks that set the $H + GG^*$ edge in $j \le 12$ on the grid of Section 4.5. The determinants and factorizations over $\mathbb{Q}$ are exact algebra, and the edge factors of $B_{1,3/2}$, $B_{2,2}$, $B_{12,7}$ and $B_{2,1}$ were checked irreducible over $\mathbb{Q}$ again by an independent rerun.

Examples of switches (computed): from $B_{3,1/2}$ to $B_{2,1}$ along $y = 0.5$ at $t = 2.304727$ (edge -0.49703); from $B_{3,1/2}$ to $B_{4,0}$ at $t = 2$, $y = 0.752443$ (edge -0.611741); from $B_{4,0}$ to $B_{1,3/2}$ at $t = 2$, $y = 1.896879$ (edge -0.699953). At $t = 3, 4, 5, 6$ the switch from $B_{2,1}$ to $B_{3,1/2}$ is at $y = 0.574998$, 0.621151, 0.650418, 0.673813, and from $B_{3,1/2}$ to $B_{4,0}$ at $y = 0.874254$, 0.930635, 0.965022, 0.988971. The closest runner-up gap is 0.0053, at $(t, y) = (2, 0.75)$. One boundary, from $B_{12,6}$ to $B_{2,1}$ along $y = 0.25$ for $t \in [2, 3]$, was not located. The smallest of these blocks has a short edge factor; for $B_{1,3/2}$ it is

$$\begin{aligned} &2s^8x - 5s^7x^2 - s^7y^2 - s^6x^3 + 7s^6xy^2 + s^5x^4 + 2s^5x^2y^2 - 23s^5x^2 - s^5y^4 + 7s^5y^2 - 3s^4x^3y^2 \\ &\quad + 9s^4x^3 + 3s^4xy^4 - 7s^4xy^2 - 30s^4x + 2s^3x^4 - 10s^3x^2y^2 + 4s^3x^2 + 6s^3y^4 + 2s^3y^2 \\ &\qquad + 20s^2x^3 - 28s^2xy^2 - 20s^2x + 56sx^2 - 40sy^2 + 48x. \end{aligned}$$

B Certificates and checks

B.1 The two slices (Theorem 5.6)

Table 4. The two slices of Theorem 5.6 (`wp3_slice_iff.json`). x_A^* is the double-precision edge of `exact_edge.json`.

	$y = \sqrt{3}$	$y = 3/2$
x^*	-0.3821684822419167	-0.37158172515020627
r_{next}	-0.0650646510788456	-0.008268340671784679
$\partial_x P_2$ on $x^* \pm 10^{-6}$	$\approx 1.1032 \times 10^7$	$\approx 8.3613 \times 10^6$
P_1 on $x^* \pm 10^{-6}$	[23434.09, 23434.34]	[20392.46, 20392.68]
smallest pivot bound, block $(1, 3/2)$	0.0038	0.027
$x^* - x_A^*$ (computed)	9.4×10^{-16}	2.4×10^{-13}

(E1) The blocks are built exactly in SymPy [24]. $B_{4,0}$ is exactly real symmetric, and the two 1×1 blocks of charge $\pm(l + 2)$ equal λ_j exactly and are set aside. The exact blocks agree

with the double-precision blocks to 2.8×10^{-14} (this is the slice part of (T)). *(E2)* On the slice, $3^9 D = P(x, y, \sqrt{3})$ with D the determinant, and the factorization $P = -16384\, P_1 P_2$ is recomputed, with degrees $(5, 6, 12)$ and $(7, 8, 16)$, both factors even in y. *(E3)* Write $P_i = A + \sqrt{3}B$ with A, B polynomials in x with rational coefficients. The norms $N = A^2 - 3B^2$ are squarefree, so every real root is simple, and rational isolating intervals of width below 4×10^{-31} are computed. In $[-3, 1]$, P_2 has one root, x^*, and P_1 has two, r_{next} and one near +0.19 (resp. +0.13). The enclosures of $\partial_x P_2$ and of P_1 on $x^* \pm 10^{-6}$ in Table 4 are bounded away from zero. *(E4)* Interval Cholesky [1] of $B_{4,0}(-3) - \lambda_4(-3)$ succeeds (smallest pivot lower bounds 30.09 and 30.40), so $m(-3) > 0$. Between -3 and r_{next} the function $\det(B_{4,0} - \lambda_4)$ vanishes only at x^*, and there simply. By the analytic dependence of the eigenvalue branches on x (Rellich), exactly one branch crosses λ_4 at x^*, and it is the lowest. A double-precision check gives $m(x^* + 10^{-3}) = -0.0110$ on both slices. *(E5)* The 116 other blocks of each slice are certified positive definite after subtracting λ_j, by interval Cholesky on $[-3, x^* + 0.02]$ with at most 14 pieces and bisection depth 2, at 96 bits in MPMATH [19]. The smallest pivot lower bound is a bound, not an eigenvalue gap; the smallest double-precision gap is 0.051 ($y = \sqrt{3}$, in the block $(1, -3/2)$) and 0.121 ($y = 3/2$) (`scripts/edge_wp3_slice_iff.py`, receipts `wp3_slice_iff.json`, `wp3_slice_iff.md`, `wp3_slice_iff_log.txt`; about 25 s, and a rerun gave an identical receipt, apart from the run time, in 24.85 s).

B.2 The slabs (Theorem 5.7)

Table 5. Boxes $x \times y \times t$ of Theorem 5.7, all sectors $j \geq 2L_0$. δ: how far the top of the box lies below the smallest value of $\min(x_{12}^*, 0)$ over the grid points of its slab (computed). Pieces: bisection pieces for the hardest blocks. Receipts `research/edge-theorem-20261121/wp2_interval_proof_*.json`.

box	L_0	δ	pieces	seconds
$[-3, -0.575] \times [0.5, 3] \times [3, 4]$	20	0.1006	498	23.1
$[-3, -0.495] \times [0.5, 3] \times [3, 4]$	20	0.0206	551	84.7
$[-3, -0.355] \times [0.5, 3] \times [4, 5]$	20	0.1010	359	19.1
$[-3, -0.274] \times [0.5, 3] \times [4, 5]$	20	0.0200	384	63.3
$[-3, -0.229] \times [0.5, 3] \times [5, 6]$	20	0.1007	404	21.0
$[-3, -0.149] \times [0.5, 3] \times [5, 6]$	20	0.0207	954	21.1
$[-3, -0.183] \times [0.5, 3] \times [6, 7]$	20	0.1002	590	24.4
$[-3, -0.103] \times [0.5, 3] \times [6, 7]$	20	0.0202	1,579	31.6
$[-3, -0.154] \times [0.5, 3] \times [7, 10]$	20	0.1005	2,892	55.7
$[-3, -0.074] \times [0.5, 3] \times [7, 10]$	20	0.0205	12,445	212.0
$[-3, -0.02] \times [1, 3] \times [7, 10]$	20	0.0196	126,082	4,445.8
$[-3, -0.6] \times [0.5, 3] \times [3, 10]$	10	0.1256	4,005	109.5
$[-3, -0.6] \times [0.5, 3] \times [3, 10]$	20	0.1256	1,653	40.5

All arithmetic is MPMATH interval arithmetic at 80 bits [19]; $N_1 = 8$ and $X_A = 20$ for $L_0 = 20$, and $N_1 = X_A = 10$ for $L_0 = 10$. The bulk rows are those with $\min(\xi, 2l - \xi) \geq N_1 - 1$. Every receipt reports `all_proved` true and the symmetry $G(l, 2l - \xi, a) = G(l, \xi, -a)$, used to reduce the bulk rows to $\xi \leq l$, checked symbolically. The excluded block of charge $-(l + 2)$ equals λ_j by Proposition 3.1 and Lemma 2.3, and its single entry is exactly λ_j on the rows (Lemma 5.8). The near-end matrices agree with the blocks to 4.5×10^{-16} (double precision). A rerun of the box $x \leq -0.6$, $L_0 = 20$ reproduced the proof in 125.7 s (receipt `wp2_verify_rerun_x-0.6_L20.json`;

design in `wp2_large_sector_bound.md`).

Exact endpoints. The proof script reads each endpoint as a binary64 double and encloses it exactly (`mpmath.mpf` of the double), so the boxes actually certified are the closed boxes whose endpoints are those doubles, which are dyadic rationals. The endpoints in y and t (0.5, 1, 3, 4, . . . , 10) and the lower endpoint $x = -3$ are exact. For the upper endpoints in x, nine of the twelve doubles lie above the decimal, so the certified box contains the box as written: -0.575, -0.495, -0.355, -0.149, -0.183, -0.103, -0.154, -0.074 and -0.6 (by between 2×10^{-18} and 4.5×10^{-17}). Three lie below the decimal, so for them the theorem holds on the box with the exact dyadic endpoint, and the sliver between it and the decimal is not certified:

- -0.274 is certified as $-0.27400000000000002131628207280300557613 37\ldots$ (a sliver of 2.1×10^{-17});
- -0.229 is certified as $-0.22900000000000000091038288019262836314738\ldots$ (a sliver of 9.1×10^{-18});
- -0.02 is certified as $-0.02000000000000000004163336342344337026588 6\ldots$ (a sliver of 4.2×10^{-19}).

Each listed value is the exact decimal expansion of the double (a dyadic rational), truncated after 40 digits. The domain D of Theorem 6.1 and the range $[2.75, 10]$ of the Floor paper have dyadic endpoints and are covered exactly.

Why plain Gershgorin is not enough near the edge. At the near end of a sector the true margin is $lK_a + O(1)$, but plain Gershgorin needs l of order $1/K_a^2$. Sampled cutoffs (double precision; not certified): at distance 0.1 below the edge $\min(x^*, 0)$, the worst grid point $(t, y) = (10, 3)$ needs $l \approx 8978$ for plain Gershgorin and $l \approx 353.5$ for a weighted Gershgorin bound with an l-dependent diagonal similarity; a direct check puts the true weighted cutoff there at 345. The cutoffs are grid-quantised estimates. The weighted bound was not turned into an interval proof; the near-end $LDL^\top$ replaced it (`wp2_bounds.json`).

B.3 The domain (Theorem 6.1)

Sectors $j \geq 80$. G is proved positive for all $l \geq 40$ on D by interval bisection, split into region A ($\xi \leq 20$) and region B ($\xi \geq 20$, with a relaxed bound). In region B the smallest lower bounds run from 0.7226 (type $(0, 0)$) to 1.5918 (type $(-1, 1)$). In region A the smallest lower bound is 1.0678×10^{-4} (type $(0, 1)$, $\xi = 0$, 1360 pieces); like the small-sector numbers below, it is the slack of a bisection stopping rule, not a spectral margin. The run takes 13.5 s. That G is exactly the diagonal minus λ minus the Gershgorin radius is Lemma 5.8; the earlier double-precision check (excess at most 2.84×10^{-13} on random rows) stays as a cross-check.

Sectors $j < 80$. D is cut into boxes. On each box the lowest eigenvalue of $B - \lambda_j I$ at the centre is bounded below by an interval $LDL^\top$ certificate with outward rounding and an a posteriori residual (`scripts/ricci_su2_outward.py`). Its variation over the box is bounded by $\sum_i \sup\|\partial_i A\|_F$ times the half-widths, with the derivatives enclosed in interval arithmetic [19]. A box whose bound is not positive is split. In all, 80 sectors and 3400 blocks were certified on 1,640,935 boxes with no failure. The summed run time is 229,134.7 s, about 63.6 CPU-hours. The interval blocks agree with the double-precision closed-form blocks to 1.7×10^{-13} (receipt

entry `point_check`); that is a check of the interval evaluation and part of (T), not a comparison with the general builder.

Rounding. The last scalar operations of each box (the centre bound minus the residual, the half-widths in s, the mean-value sum, and their difference) are done in 64-bit round-to-nearest, not in directed rounding. The box endpoints are dyadic with at most 25 bits, so the half-widths in x and y are exact. An a priori error analysis bounds the total error by $\kappa(1+u)M^* = 1.63 \times 10^{-15}$, with $u = 2^{-64}$, $\kappa = 2.71 \times 10^{-19}$, and $M^* = 6025.62$ an interval bound on the centre value over D (attained at $j = 79$). The smallest certified lower bound is 1.2220726×10^{-6}, 7.48×10^8 times larger, so no verdict can change (`scripts/ricci_su2_family_cert_rounding_bound.py`, receipts `rounding_bound.json` and `rounding_bound.md` in `P`). The receipt stores only the minimum per sector, so a directed recheck of its own boxes would mean rerunning the certificate. As a demonstration, a directed version of the final combination agrees with the code as written on 60 random sub-boxes (45 certified), and its value is never above the round-to-nearest one.

Table 6. The small-sector certificate of Theorem 6.1: the sector $j = 0$, the four sectors with the smallest certified lower bounds, and the total (`family_block_cert_j80.json`). The lower bounds are box slack, set by the stopping rule of the bisection; the actual margin on D is about 2.35 or more (Remark 6.3).

sector	boxes	smallest certified lower bound (box slack)	seconds
$j = 0$	11,431	1.41×10^{-4}	400.0
$j = 1$	71,052	1.2220726×10^{-6}	3,152.2
$j = 2$	71,729	2.94×10^{-5}	5,360.8
$j = 3$	54,736	5.77×10^{-6}	5,501.7
$j = 36$	14,015	6.90×10^{-5}	2,103.3
$j = 0, \ldots, 79$	1,640,935	1.2220726×10^{-6}	229,134.7

B.4 Positive x and the near-top families

A worked example (double precision, except the threshold). At $(x, y, t) = (0.1, \sqrt{10}, 10)$ the type $(1, -1)$ has $K = -0.252982212813$ and constant term 38.4821067231, so by Theorem 5.1 the twist loses in every sector with $l > 152.113883008$. The type $(1, 0)$ has $K = -0.126491106407$ and constant term 29.2310533616, and loses for $l > 231.091767571$. The actual undercut comes earlier, because the lowest eigenvalue of a block is below its diagonal. From the blocks, the margin $\min_q \lambda_{\min}(B_{j,q}) - \lambda_j$ is -0.58346 at $j = 120$ (minimising charge $q = -61$), -8.9498 at $j = 200$ and -34.100 at $j = 400$. An independent full-sector builder gives -0.583 for $H + GG^*$ and -0.581 for the gauge-orthogonal spectrum at $j = 120$, and -8.95 at $j = 200$ (`research/edge-theorem-20261121/wp2_large_sector_bound.md`, Section 0, and the verifier's rerun in `workflow_reports.json`).

Near $x = 0$ (double precision; not certified). At $(t, y) = (10, \sqrt{10})$ and $x = 0$ the margin stays positive and rises slowly: 7.7516 at $j = 2000$ and 7.7752 at $j = 20000$. At $x = +0.01$ it is negative at large j: -7.67 at $j = 2000$ and -32.9 at $j = 4000$ (`workflow_reports.json`). The margin at the near end of each sector is of order one at $x = 0$. No proof here covers $x \in (-0.02, 0)$.

The positive edges of the cut-off. At all 58 grid points of the competitor map with $x_{12}^* > 0$, some sector $j > 12$ undercuts the twist at x_{12}^*: at 54 points within $13 \le j \le 200$ (`wp1_tail_check.json`,

near-top charges only), and, in the verifier's rerun, at $(7, 2.0)$, $(7, 2.25)$ and $(7, 2.5)$ by the sectors $j = 2000$, 400 and 400, and at $(12, 3)$ by $j = 100$, with margin -10.46. In a full charge scan at four of these points the minimising charge was $|q| = l + 1$ or l. Table 7 shows how the edge falls as the cut-off J is raised at one point. In the other direction, at $x = -0.01$ and $x = -0.001$, at each of the 57 positive-edge points of the tail run (all but $(12, 3)$), neither the near-top blocks of $13 \le j \le 2000$ nor any block of $j \le 12$ undercuts the twist; the smallest margin is 0.029 (`wp1_tail_check.json`, `wp1_tail_negx.json`, `wp1_fullsector_check.json`, `workflow_reports.json`).

Table 7. The edge of the sectors $j \le J$ at $(t, y) = (12, 2.75)$ (double precision; `wp1_competitor_map.md`, Section 4).

J	12	24	48	96	192
edge	0.1825	0.1825	0.1706	0.0969	0.0519

Table 8. Edge of the near-top family $q = l + 1$ at $(t, y) = (12, 2)$ (double precision; receipt `wp1_competitor_map.md`, Section 4).

j	12	24	48	96	200	400	1000	2000
edge	0.2075	0.1458	0.0905	0.0513	0.0264	0.0137	0.0056	0.0028

B.5 Lean theorems

`Helike/Edge.lean` (four theorems). The polynomials are those of the receipt `edge_polynomial.srepr`; the 473-term determinant is entered in ten parts of at most 48 terms, checked equal to the receipt by sympy before the Lean was written.

- `edgeDet_factor`: for all real x, y, s, `edgeDet` $= -16384\, P_1 P_2$.
- `edgeFactor_berger`: for $s \neq 0$, $P_2((2 - s^2)/s, s, s) = -32(s - 1)(s + 1)Q_{16}(s)$.
- `tA_poly_root`: Q_{16} has a root $s \in [1.65261, 1.65262]$, by the intermediate value theorem ($Q_{16}(1.65261) < 0 < Q_{16}(1.65262)$).
- `berger_crosses_edge`: there is $s \in [1.65261, 1.65262]$ with $P_2((2 - s^2)/s, s, s) = 0$ and $s^2 \in [2.73111, 2.73116]$.

`Helike/Price.lean` (twelve theorems). With $t = s^2$, $s \neq 0$, the closed form (4) is `price`, κ is `kappa`, B is `fieldCurv`, and $\lambda_t(j)$ is `floorLaw` $t\ j = (j^2 + (8 - 2t)j - 2t^2 - 4t + 16)/t$. The theorems are `price_anatomy` (item (4) of Proposition 3.4, as an algebraic identity); `floorLaw_paper_form`; `kappa_berger`, `fieldCurv_berger` and `price_berger` (the Berger slice, and $\lambda = \lambda_t(j)$ there); `floorLaw_three`, `floorLaw_three_sector0` ($-14/3$) and `floorLaw_three_sector12` ($154/3$) at $t = 3$; `floorLaw_vertex_form`, $\lambda_t(j) = (j - (t - 4))^2/t + (4 - 3t)$, with `floorLaw_ge_vertex` and `vertex_on_line`; and `floorLaw_cutoff`, $\lambda_t(t - 4 + \sqrt{t(3t - 4)}) = 0$ for $t \ge 4/3$.

The builds completed on two machines (Price: 18254 jobs; a full rebuild: 18256 jobs, with `Helike.Edge` taking 231 s for the factorization, of degree 28 in s).

C Pre-registration details

Each test's documents are in `research/edge-theorem-20261121/`: `wp4_prereg_A_heldout.md` (with `wp4_prereg_A_points.json`), `wp4_prereg_B_general_fields.md` and `wp4_prereg_C_su3.md`; Test D is in `research/edge-theorem-20261122-d/wp5_prereg_D_su3_own_circle.md`; Test E in `research/edge-theorem-20261122-e/wp6_prereg_E_two_hands.md`; Test F in `research/edge-theorem-20261122-f/wp7_prereg_F_principal_circle.md` with its two amendments (`wp7_prereg_F_amendment1_peak.md`, `wp7_prereg_F_amendment2_wall.md`); the registered, still running Test G in `research/edge-theorem-20261122-g/wp8_prereg_G_two_new_groups.md`.

C.1 Test A

Points. 48 points (t, y), drawn with seed 20261121: 30 in the class where P_2 governs ($t \sim U[2.2, 11.5]$, $y \sim U[1.1, 3.2]$), 10 at small y ($y \sim U[0.3, 0.7]$), and 8 on a fixed grid ($t \in \{2.2, 3.5, 7.0, 11.0\}$, $y \in \{1.2, 2.5\}$). None lies within 10^{-3} of the 50 pairs (t, y) used before.

Predictions. A1: the edge is a root of P_2, with competitor $B_{4,0}$, at the 38 points outside the small-y class. A2: at small y the competitor is a block of the sector $j = 2$ or 3. A3: no sector $13 \le j \le 79$ undercuts the twist at three values of $x < 0$ (just below $\min(x^*, 0)$, at the midpoint of the region, and just above x_{lo}); $x > 0$ is excluded, since the undercut there is proved. A4: on a 0.01 grid over $[r_{\mathrm{lo}} - 0.5,\ x^* + 0.5]$ the region of the sectors $j \le 12$ is a single interval.

Measurement and gates. The edge is measured on an independent code path, the full $H + GG^*$ sector, with both copies of λ_j removed. Gates: A-code-1 (blocks against the full spectrum, 10^{-12} relative); A-code-2 (18 known rows to 10^{-9}); A-code-3 (the Berger path at t_A, 10^{-8} relative); A-mult (exactly two eigenvalues at λ_j); A-branch (the largest real root of P_1 must miss the measured edge by more than 10^{-6} at no fewer than 80% of the P_2-class points, or A1 is inconclusive); A-bound ($x_{\mathrm{lo}} \ge r_{\mathrm{lo}}$); A-bound-hi ($x^* \le r_{\mathrm{hi}}$). Verdict rule: A1 is supported if it holds at all 38 points, and a failure counts against the edge clause; a failure of A3 counts against the claim for $x < 0$; a hole in A4 counts against the interval. Three caveats were written down in advance. A1 agreement is partly automatic, because P_2 comes from the same closed-form rows that A-code-1 checks. "Held-out" means not yet computed. The claims cover $j \le 79$ only.

Amendment 1. Gate A-code-3 passed (relative residual 1.0×10^{-18}). Gate A-code-2 fired, with maximum deviation 3.67. On the 18 known rows alone, P_2 was recovered exactly (degrees $(7, 8, 16)$, 113 terms) and the edge is a real root at every row, but not the largest root in $[-3, 3]$. P_2 has three or four further real roots above the edge, where a higher eigenvalue of $B_{4,0}$ meets λ_4. The rule was amended: the predicted edge is the largest real root r of P_2 in $[-3, 3]$ at which the lowest eigenvalue of $B_{4,0}(r, y, t)$ equals $\lambda_4(r)$ to $10^{-8} \max(1, |\lambda_4|)$; if there is none, A1 fails there. A-branch uses the same selection for P_1. Nothing else changed. The known-answer rows thus count against the statement "the edge is the largest real root of P_2".

Gate values. A-code-1 to 4.1×10^{-15}; A-code-2 with 113 terms and the 18 known rows to 2.4×10^{-13} under Amendment 1; A-code-3 to 1.0×10^{-18}; A-mult at every point and sector $j \le 12$; A-bound and A-bound-hi, with $x_{\mathrm{lo}} - r_{\mathrm{lo}} \ge 1.61$ everywhere; A-branch at 100% of the P_2-class points.

Table 9. The four points where A1 failed.

t	y	predicted (root of P_2)	measured	competitor
2.295	2.687	−0.6089	−0.6941	$(1, -\frac{3}{2})$
2.2	2.5	−0.6378	−0.7148	$(1, -\frac{3}{2})$
3.5	2.5	−0.2979	−0.3202	$(1, -\frac{3}{2})$
11.0	1.2	+0.0847	+0.0736	$(12, -7)$

The map of Section 4.5 already showed $(1, \pm\frac{3}{2})$ for $y \geq 2$ and $t \leq 4$, and the P_2-class box of Test A overlapped that corner. The statement "for $y \gtrsim 1$ the edge is the root of P_2" is therefore counted against.

C.2 Test B

B-I, a code control. 200 members are drawn (generator seed 1122, weight $k = \pm 1$, $x \sim U[-10, 10]$, $y \sim U[0, 6]$, $z \sim U[-6, 6]$, $t \sim U[0.5, 15]$, a random constant gauge frame), sectors $j \leq 8$. Gates: B-sym, B-exact, B-red (the twist's value equals λ at the reduced coordinates to 10^{-10} relative), B-spec (full spectra equal those of the reduced field to 10^{-12} relative) and B-even (10 extra draws at $y = z = 0$).

B-II, the part that can fail. A random scan of the reduced family over (ρ, t) at the 200 reduced draws, with x and k discarded and the edge located on $x \in [-10, 10]$ in $j \leq 12$. Gates: B-II-code (the 27 rows of `exact_edge.json` reproduced to 10^{-9}); B-count (at least 60 scored points, or B-S and B-half are inconclusive); B-S (the competitor's slope ratio below 0.5 at every scored edge; the threshold was chosen after seeing ratios 0.16, 0.064 and 0.165); B-half (exactly two sign changes of ϕ_A on a 0.01 grid over $[r_{\text{lo}} - 0.5,\ x^* + 0.5]$); B-N, the competitor's charge, descriptive only.

Amendment B1. Gate B-II-code stopped the run before any B-II point was computed. At all 27 known rows the edge was reproduced (largest deviation about 4×10^{-15}), but at two rows ($t = 3$ and $t = 4$, height 0.5) the competitor was read as $(2, +1)$ where the receipt has $(2, -1)$, and the reverse. At every known row whose competitor has $q \neq 0$, the blocks (j, q) and $(j, -q)$ have the same lowest eigenvalue to 6.7×10^{-15} (double precision), and which one is reported is decided by rounding. The gate was amended to accept the competitor up to $(j, q) \leftrightarrow (j, -q)$ when the two lowest eigenvalues agree to 10^{-12} relative at $x^* + 10^{-4}$. The scored arms are unaffected: B-N asks whether $q = 0$, B-S uses a slope that the mirror shares, and B-half does not use the competitor. The final receipt `wp4_general_fields.json` records the protocol "`wp4_prereg_B_general_fields.md` @ 232ab8d + Amendment B1" and `B_II_code` true.

C.3 Test C

The family. The left-invariant fields commuting with the joint frame-and-gauge action of $U(2)$ form a space of dimension 4 (computed by SVD to machine precision). Components are in the orthonormal coframe. The Maurer–Cartan member $u = y = \frac{1}{2}$, $x = 1/(2\sqrt{t})$ is the field of the second $SU(3)$ family of Section 7, where the extremal state was the floor nowhere. The analogue of the twist has charge $q_8 = \sqrt{3}/2$ under the fibre generator. Three structural statements were labelled conjectures until their gates pass: F1, the coefficient of x^2 in its eigenvalue is $q_8^2 = 3/4$ in every sector; F2, its region in x is bounded, via the gauge-orthogonal state $\hat{\theta}^8 \otimes X_8$ of the sector

$(0,0)$, whose Rayleigh quotient is affine in x; F3, the lift discount is linear in x with one sign σ across the sectors.

Predictions. C-P1, existence: with x free, the region where the twist is the floor of all nine sectors (gauge-orthogonal spectrum) is non-empty, strictly at every grid point with $t \geq 3$, weakly at one point at least. C-P2, side: at every informative point the midpoint of the region satisfies $\sigma x < 0$. C-P3: the region is one interval. C-P4: at the upper edge the competitor's slope ratio is below 0.5 (scored); its charge is descriptive. C-P5: the upper edge against t, descriptive. Every claim of Test C is about the nine listed sectors, and a region narrower than the step 0.25 cannot be seen.

Gates. C-K1 to C-K5 (the earlier $SU(3)$ controls, an $SU(2)$ analogue against `exact_edge.json`, and a known answer at the Maurer–Cartan member), C-sym, C-quad (second difference 3/2 to 10^{-9}), C-lin, C-sigma, C-mult and C-bound. Values: C-K1 to C-K3 passed; C-K4 coefficient of x^2 equal to 1 to 3×10^{-14} and three known edges to 3×10^{-9}; C-K5 to 2.6×10^{-14}; C-sym ($\|[Q, H]\|$ to 1.1×10^{-14} relative, residual of the twist 8×10^{-16}, $\|G^* b\|$ 7×10^{-16}); C-quad at all 20 shapes and nine sectors to 9×10^{-15}, so F1 holds; C-lin exactly, so F2 holds; C-sigma with $\sigma = +1$ everywhere; C-mult under Amendment C2, with the extra tied doublet at the five shapes $(u, y) = (\frac{1}{2}, 1)$.

Amendment C1. A smoke test of the structure gates at one shape point, $(t, u, y) = (8, 1, 2)$, was run before any floor, edge or competitor was computed. C-quad passed (3/2 to 5.3×10^{-15} in all nine sectors), C-lin passed (second difference 0.0), $\sigma = +1$, and $[r_{\text{lo}}, r_{\text{hi}}] = [-7.656, 4.120]$. Gate C-mult would have stopped the run: the number n_b of slice eigenvalues equal to the twist's value was 6, 4, 8, 5, 5, 6, 10, 6, 7 in the sectors $(0,0)$, $(1,0)$, $(1,1)$, $(2,0)$, $(2,1)$, $(3,0)$, $(2,2)$, $(3,1)$, $(4,0)$, not 1 or 2. The family commutes with a non-abelian $U(2)$, so eigenvalues come in multiplets of its $SU(2)$; the twist has spin $p/2 + 1$ there, and the count is $n_b = (p + 3)$(2 if $p = q$, else 1), which matches all nine. This formula was derived after seeing the counts. The amended gate requires that count and removes exactly n_b copies. The predictions C-P1 to C-P5 are unchanged.

Amendment C2. The rerun passed C-K1 to C-K5 again, and the shape point $(2, \frac{1}{2}, \frac{1}{2})$ passed every structure gate. At $(2, \frac{1}{2}, 1)$ the amended C-mult stopped the run: the counts were 6 in $(1,0)$, where the formula gives 4, and 12 in $(1,1)$, where it gives 8, the same at all three x values. The extra states form a second $SU(2)$ doublet, with charges 3 and 4, outside the twist's multiplet, whose eigenvalue equals the twist's identically in x at $(u, y) = (\frac{1}{2}, 1)$; this was seen at $t = 2$, 2.0001 and 3, and not at the other shapes examined. They are tied competitors, not copies of the twist. The gate was amended again: n_b must be at least the multiplet count and the same at the three x values, exactly the multiplet count is removed, and any further states at the twist's value stay in the spectrum as competitors. Under the registered non-strict floor rule a tie leaves the twist the floor; where the extra counts are identical in x the twist is never the unique floor in that sector. In the same amendment the spectra were moved, as an implementation change, to the eigenbasis of the field-independent charge, block by block (a unitary change of basis, agreeing with the dense computation to 2×10^{-13} on the largest sector). No floor, edge or competitor had been computed.

C.4 Test D

Family. $SU(3)$ with $X_a = -(i/2)\lambda_a$ and $\langle X, Y\rangle = -2\,\mathrm{tr}\,XY$; orthonormal Cartan basis $e_H = \frac{1}{2}X_3 + \frac{\sqrt{3}}{2}X_8$, $e_K = \frac{\sqrt{3}}{2}X_3 - \frac{1}{2}X_8$; metric t on e_H and 1 on the other seven. The left-invariant fields commuting with the joint frame-and-gauge action of the torus form a space of dimension 10; the registered five-parameter sub-family is $M_{e_H} = x\,e_H$, $M_{e_K} = w\,e_K$, and y_{12}, y_{23}, y_{13} times the identity on the three root planes. The twist is the highest weight times $E_\theta \otimes E_\theta$, with charge $p + q + 4$ under the joint circle of H. The grid is $t \in \{2, 3, 4, 6, 8\}$ and $(w, y_{12} = y_{23}, y_{13}) \in \{(\frac{1}{2}, \frac{1}{2}, \frac{1}{4}), (\frac{1}{2}, \frac{1}{2}, \frac{3}{4}), (\frac{1}{2}, 1, 1), (1, 1, \frac{3}{2})\}$, with the nine sectors of Test 2; y_{13} maps to the $SU(2)$ heights 0.5, 1.5, 2, 3.

Predictions and gates. D-P1, existence (weak and strict). D-P2, side, in its revised form: the floor set lies in $\{\sigma x \le 0\}$, scored only where $\sigma r_{\mathrm{hi}} > 0$ and where an $SU(2)$ calibration run at the same shape has a non-positive upper edge; if no shape is scorable, D-P2 is not informative. D-P3, one interval. D-P4, the competitor's slope ratio below 0.5 (post hoc). D-P5, descriptive. Gates D-K1 to D-K7 (the Test C controls, a rotated-basis control at $t = 1$, and a wrong-axis control reproducing Test 2b), D-sym, D-quad (second difference 2), D-lin, D-sigma (structural, not evidence), D-kappa, D-mult (exactly the twist and its mirror removed; other ties kept as competitors), D-bound, and D-ext (two further sectors evaluated wherever the floor set is non-empty; a pass of D-P1 without them is reported as truncation-sensitive). Wherever the grid finds no region, a golden-section search on ϕ_S runs to 10^{-6} in x, so that a narrow region is not missed.

Verdict rule and status. A failure of weak D-P1 counts against the reading in this $SU(3)$ slice, even along the twist's own circle; a failure of D-P2 where informative counts against "turns against her charge" in $SU(3)$; a failure of D-P3 against the interval form; a failure of D-P4 against "nearly blind". If all hold, the reading is supported in one $SU(3)$ family, in nine sectors, which would itself be a hypothesis for a further test. The verdict is scoped to this slice (diagonal Cartan block, zero phases, $y_{12} = y_{23}$), these shapes and these sectors. The design was revised after an adversarial review, before any floor, edge or competitor was computed. The results are reported in Section 8: D-P1 (weak and strict), D-P2 and D-P3 held; D-P4 failed.

References

[1] G. Alefeld, G. Mayer, The Cholesky method for interval data, *Linear Algebra Appl.* 194 (1993) 161–182, doi:10.1016/0024-3795(93)90120-D.

[2] I. G. Avramidi, S. Collopy, Thermal Yang–Mills theory in the Einstein universe, *J. Phys. A* 45 (2012) 374009, doi:10.1088/1751-8113/45/37/374009, arXiv:1201.5163.

[3] C. Bär, The Dirac operator on homogeneous spaces and its spectrum on 3-dimensional lens spaces, *Arch. Math.* 59 (1992) 65–79, doi:10.1007/BF01199016.

[4] S. Bolognesi, C. Chatterjee, S. B. Gudnason, K. Konishi, Vortex zero modes, large flux limit and Ambjørn–Nielsen–Olesen magnetic instabilities, *JHEP* 10 (2014) 101, doi:10.1007/JHEP10(2014)101, arXiv:1408.1572.

[5] J.-P. Bourguignon, H. B. Lawson, Stability and isolation phenomena for Yang–Mills fields, *Comm. Math. Phys.* 79 (1981) 189–230, doi:10.1007/BF01942061.

[6] B. R. Davis, The Floor Theorem for the Yang–Mills Hessian at the Berger field: a floor law across the Berger spheres, 2026, `https://doi.org/10.5281/zenodo.24412603` (concept DOI 10.5281/zenodo.24386613).

[7] B. R. Davis, Reading the curve, not counting the points: a two-ring Petrov–Galerkin curvature force for discrete Yang–Mills dynamics on the Poincaré homology sphere, 2026, `https://doi.org/10.5281/zenodo.24328085`.

[8] F. D. M. Haldane, Fractional quantization of the Hall effect: a hierarchy of incompressible quantum fluid states, *Phys. Rev. Lett.* 51 (1983) 605–608, doi:10.1103/PhysRevLett.51.605.

[9] X. Han, Y. Wen, Nonexistence of weakly stable Yang–Mills fields, 2026, arXiv:2601.17649.

[10] J. Henkel, E. A. Lauret, Hodge Laplacian on 1-forms of homogeneous 3-spheres, 2026, arXiv:2605.05406.

[11] X. Jin, Stable abelian Yang–Mills–Higgs fields on the round three-sphere, 2026, arXiv:2609.24045.

[12] K. Kumar, O. Lechtenfeld, G. Picanço Costa, Instability of cosmic Yang–Mills fields, *Nucl. Phys. B* 973 (2021) 115583, doi:10.1016/j.nuclphysb.2021.115583, arXiv:2102.08401.

[13] J. Kling, D. Schueth, On the Dirac spectrum of homogeneous 3-spheres, *J. Geom. Anal.* 32 (2022), no. 11, Paper No. 175, doi:10.1007/s12220-022-00997-x, arXiv:2204.12990.

[14] S. Kobayashi, Y. Ohnita, M. Takeuchi, On instability of Yang–Mills connections, *Math. Z.* 193 (1986) 165–189, doi:10.1007/BF01174329.

[15] H. T. Laquer, Stability properties of the Yang–Mills functional near the canonical connection, *Michigan Math. J.* 31 (1984) 139–159, doi:10.1307/mmj/1029003019.

[16] E. A. Lauret, The smallest Laplace eigenvalue of homogeneous 3-spheres, *Bull. Lond. Math. Soc.* 51 (2019) 49–69, doi:10.1112/blms.12213, arXiv:1801.04259.

[17] L. de Moura, S. Ullrich, The Lean 4 theorem prover and programming language, in *Automated Deduction – CADE 28*, Lecture Notes in Comput. Sci. 12699, Springer, 2021, 625–635, doi:10.1007/978-3-030-79876-5_37.

[18] The mathlib Community, The Lean mathematical library, in *Proc. 9th ACM SIGPLAN Int. Conf. Certified Programs and Proofs (CPP 2020)*, 2020, 367–381, doi:10.1145/3372885.3373824.

[19] The mpmath development team, mpmath: a Python library for arbitrary-precision floating-point arithmetic, `https://mpmath.org`.

[20] N. K. Nielsen, P. Olesen, An unstable Yang–Mills field mode, *Nucl. Phys. B* 144 (1978) 376–396, doi:10.1016/0550-3213(78)90377-2.

[21] Y. Ohnita, Y. L. Pan, On weakly stable Yang–Mills fields over positively pinched manifolds and certain symmetric spaces, *Kodai Math. J.* 13 (1990) 317–332, doi:10.2996/kmj/1138039277.

[22] G. K. Savvidy, Infrared instability of the vacuum state of gauge theories and asymptotic freedom, *Phys. Lett. B* 71 (1977) 133–134, doi:10.1016/0370-2693(77)90759-6.

[23] M. Stern, Geometry of minimal energy Yang–Mills connections, *J. Differential Geom.* 86 (2010) 163–188, doi:10.4310/jdg/1299766686, arXiv:0808.0667.

[24] A. Meurer et al., SymPy: symbolic computing in Python, *PeerJ Comput. Sci.* 3 (2017) e103, doi:10.7717/peerj-cs.103.

[25] N. Tanji, K. Itakura, Schwinger mechanism enhanced by the Nielsen–Olesen instability, *Phys. Lett. B* (2012), doi:10.1016/j.physletb.2012.05.043, arXiv:1111.6772.

[26] R. S. Varga, Geršgorin-type eigenvalue inclusion theorems and their sharpness, *Electron. Trans. Numer. Anal.* 12 (2001) 113–133.

[27] J. von Neumann, E. Wigner, Über das Verhalten von Eigenwerten bei adiabatischen Prozessen, *Phys. Z.* 30 (1929) 467–470.

[28] T. T. Wu, C. N. Yang, Dirac monopole without strings: monopole harmonics, *Nucl. Phys. B* 107 (1976) 365–380, doi:10.1016/0550-3213(76)90143-7.